Original Article

Author for correspondence:
Ruaridh Y. Smith, Email: ruaridh.smith@fau.de

CAMBRIDGE
UNIVERSITY PRESS

Using fractured outcrops to calculate permeability tensors: implications for geothermal fluid flow and the influence of seismic-scale faults

Ruaridh Y. Smith[1] , Martin Lesueur[2], Ulrich Kelka[3], Thomas Poulet[3] and Daniel Koehn[1]

[1]Geozentrum Nordbayern, Friedrich-Alexander Universität (FAU), Erlangen-Nürnberg, Germany; [2]School of Earth Sciences, University of Western Australia, Perth, Australia and [3]CSIRO Mineral Resources, Kensington WA, Australia

Abstract

Faulted and fractured systems form a critical component of fluid flow, especially within low-permeable reservoirs. Therefore, developing suitable methodologies for acquiring structural data and simulating flow through fractured media is vital to improve efficiency and reduce uncertainties in modelling the subsurface. Outcrop analogues provide excellent areas for the analysis and characterization of fractures within the reservoir rocks where subsurface data are limited. Variation in fracture arrangement, distribution and connectivity can be obtained from 2D fractured cliff sections and pavements. These sections can then be used for efficient discretization and homogenization techniques to obtain reliable predictions on permeability distributions in the geothermal reservoirs. Fracture network anisotropy in the Malm reservoir unit is assessed using detailed structural analysis and numerical homogenization of outcrop analogues from an open pit quarry within the Franconian Basin, Germany. Several events are recorded in the fracture networks from the Late Jurassic the Alpine Orogeny and are observed to be influenced by the Kulmbach Fault nearby with a reverse throw of 800 m. The fractured outcrops are digitized for fluid flow simulations and homogenization to determine the permeability tensors of the networks. The tensors show differences in fluid transport direction where fracture permeability is controlled by orientation compared to a constant value. As a result, it is observed that the orientation of the tensor is influenced by the Kulmbach Fault, and therefore faults within the reservoirs at depth should be considered as important controls on the fracture flow of the geothermal system.

1. Introduction

Faults and fractures are abundant discontinuity features in rocks that govern fluid flow in the subsurface (Caine *et al.* 1996; Sibson, 1996; Curewitz & Karson, 1997; Connolly and Cosgrove 1999; Sanderson & Zhang, 2004; Kurz *et al.* 2008; Zhang *et al.* 2008; Bense *et al.* 2013; Morley & Nixon, 2016; La Bruna *et al.* 2021; Pisani *et al.* 2022). These structural features develop at a variety of scales from large-scale regional faults to outcrop scale, fracture and stylolite networks, all of which can either enhance or impede flow in the subsurface (Caine *et al.* 1996; Odling *et al.* 1999; Bour *et al.* 2002; Sanderson & Zhang, 2004; Manzocchi *et al.* 2010; Bense *et al.* 2013; Bruna *et al.* 2019; Giuffrida *et al.* 2019; Araújo *et al.* 2021). Analysing these networks and characterizing their impact on flow and transport, is paramount for a variety of subsurface applications, e.g. geothermal energy extraction (Lipsey *et al.* 2016; Vidal *et al.* 2017; Smeraglia *et al.* 2021), hydro-carbon production (Nelson, 2001), mineral exploration (e.g. Cox, 1999), CO_2 sequestration (CSS; e.g. Stork *et al.* 2015) and hydrogen storage (Saxena *et al.* 2018). This is especially important in geothermal reservoirs where host-rock permeability is generally low, e.g. granite geothermal systems (Wibberley & Shimamoto, 2002), and fluid flow is controlled at first order by fracture network geometry (Hollinsworth *et al.* 2019).

Efficient discretization and simulation techniques are required to obtain reliable prediction of permeability distributions within geothermal reservoirs. We use a field example from an open pit quarry near Kulmbach, Germany, to show how fracture network anisotropy in geothermal reservoirs can be assessed using detailed analysis of outcrop analogues. Specifically, we analyse variation of fracture networks in a cross-section towards the seismic-scale Kulmbach Fault. We present the results of the structural analysis, followed by introducing a mixed-dimensional approach for quick discretization of the network for the numerical analysis of flow in the dense fracture networks. Based on our field data we will demonstrate the importance of linking geological field work to numerical model development. Finally, we propose a new approach to numerical permeability homogenization that is informed by detailed field observations.

1.a. Two-dimensional fracture modelling from surface analogues

Fracture spatial arrangement and variations can be quantified from several data sources at different dimensions such as 1D – scan lines (Priest & Hudson, 1981), boreholes (e.g. Rajabi *et al.* 2010) – 2D – drone imagery, pavement analysis (Boersma *et al.* 2019; Smith, 2020) – and 3D – seismic analysis (Jaglan, *et al.* 2015), lidar (Pontes *et al.* 2021), ground-penetrating radar (Grandjean and Gourry, 1996; Elkarmoty *et al.*, 2018) or outcrop mapping (Jones *et al.* 2009). Subsurface data allow for larger-scale faults (e.g. seismic surveys) and fractures (e.g. well logs) to be imaged directly from reservoirs which can be implemented into models of the fractured networks at depth (e.g. Boersma *et al.* 2021). For geothermal exploration, acquiring reliable subsurface data can be too costly, and, with the resolution limitations of seismic data, small-scale fracture networks are often overlooked (Lei *et al.* 2017). Therefore, surface fractured features can be useful for quantifying fractured networks, in particular the smaller networks, and making predictions at depth (Welch *et al.* 2015; Gutmanis *et al.* 2018).

Geological analogues are a tool for generating representations of the subsurface from outcrops and reduce uncertainty in developing geological and dynamic models (Pringle *et al.* 2006; Howell *et al.* 2014). Analogues provide information on the structure of units and fracture systems in place within formations and larger-scale regions where geologists can directly see features in the rocks. Interpreting and utilizing analogues is therefore vital for understanding the fractured networks at depth. For reservoir analogues, scan lines (1D) and fractured pavements (2D) are the most used data techniques and, whilst scan lines can provide statistical information on fracture arrangement, they are not useful for developing further models (Priest and Hudson, 1976; Dershowitz *et al.*, 1992; Prabhakaran *et al.* 2021). Two-dimensional pavement and fracture trace analysis allow for the interpretation and modelling of geometric and topological data (fracture orientation, length, intersections, aperture) from the fracture networks using advanced techniques of data acquisition, e.g. monopod and drone photogrammetry (Bisdom *et al.* 2017; Prabhakaran *et al.* 2019, Smith, 2020; Lopes *et al.* 2022).

There are several software solutions that can be used to analyse and capture data within the fractured pavements and 2D outcrops (e.g. Hardebol & Bertotti, 2013; Healy *et al.* 2017). These enable the simplification of fracture networks and focus on important parameters such as orientation, connectivity and aperture. Whilst these programs are excellent in producing statistical data on the fracture patterns, they do not provide the functionality to prepare the fracture networks for numerical modelling through the formation of fracture meshes and the clustering of fracture sets.

1.b. Numerical modelling of fractured networks

The analysis and interpretation of fracture networks provides a base from which predictions can be made of the fracture distribution on the surface and within the subsurface. However, to quantify how the fractures affect fluid flow, numerical modelling is required to obtain data that represent the flow response of the fractured network (e.g. permeability tensors; Zhang *et al.* 1996).

Integrating a fractured network into fluid flow simulations can be difficult due to the variability of fracture properties (e.g. length, orientation, aperture), but methods exist to bridge these uncertainties between sca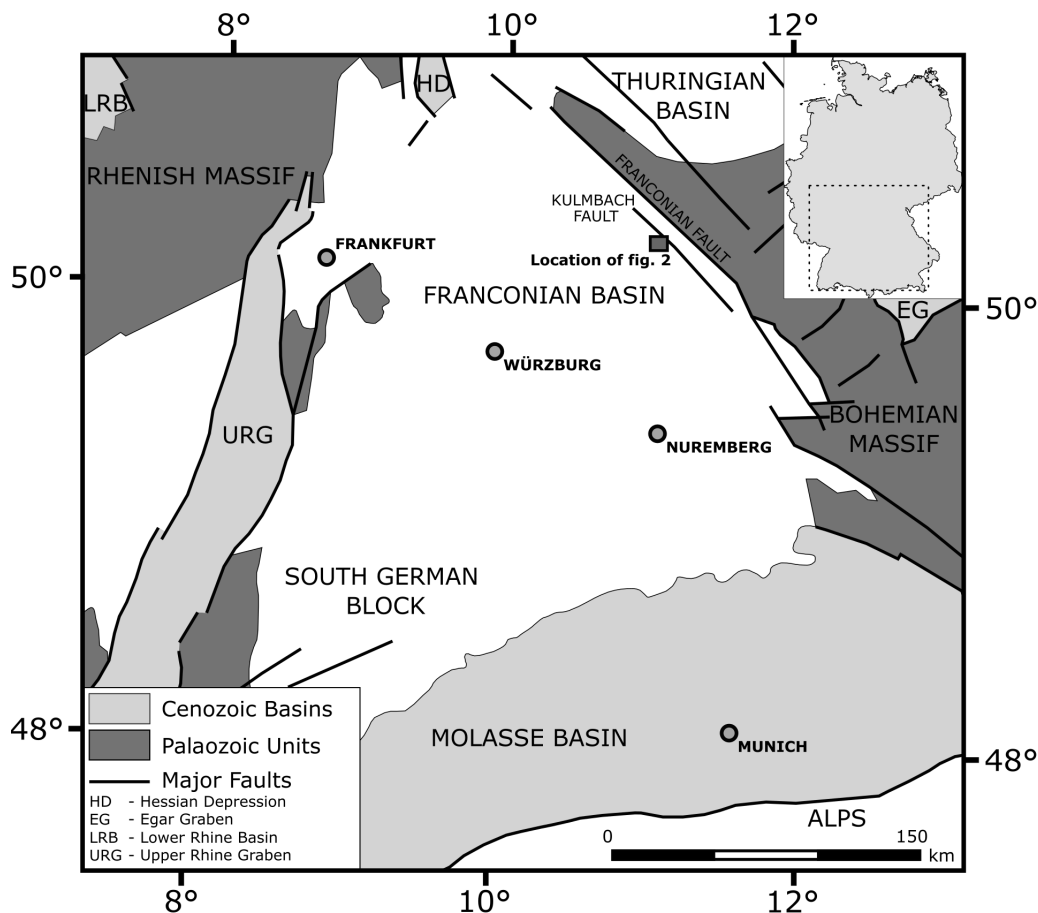les of the fractures and represent the network properties at a multiscale level (Bonnet *et al.* 2001; Liu *et al.* 2016; Berre *et al.* 2019).

Explicitly representing fracture networks within large-scale simulations poses significant computational challenges. Homogenization of the fractures provides a suitable process to integrate the small-scale networks within these simulations (Berkowitz, 1995; Geers *et al.* 2017; Thovert *et al.* 2017; Berre *et al.* 2019). It is important to accurately homogenize the fractures, as high-density networks (large-scale) effectively act as completely permeable media, and at the small scale fewer fractures will not represent the network (Fourno *et al.* 2013; Meier *et al.* 2018; Poulet *et al.* 2021).

Fracture networks within reservoirs represent thin features which can be computationally costly to discretize due to the required number of elements in the mesh. Newly developed techniques have allowed for the simulation of fractures as flat features (lower-dimensional elements) such that the fracture aperture is not considered within the mesh but instead is accounted for numerically (e.g. Alboin *et al.* 2002; Nordbotten *et al.* 2018; Poulet *et al.* 2021). By considering the fractures as lower-dimensional elements within the mesh, the required number of elements is reduced, resulting in a more efficient simulation (Cacace & Jacquey, 2017; Poulet *et al.* 2021).

An important property in simulating flow through fractured networks is fracture permeability. Faults and fractures can be conceptualized as conduits, barriers or combined conduit–barriers to fluid flow depending on various parameters such as hydraulic or mechanical variations and interactions (Caine *et al.* 1996; Poulet *et al.* 2021). Whilst fractures can be exclusively barriers (closed) or conduits (open), many natural fractures present characteristics that are between the end-members, forming conduit–barrier systems with variable permeabilities (Caine *et al.* 1996; Korneva *et al.* 2014; Bauer *et al.* 2016; Volatili *et al.* 2019; Giuffrida *et al.* 2020). For example, strike-slip faults can comprise filled cores surrounded by distributed small-scale damage zones with variable permeabilities (Mitchell & Faulkner, 2009). Techniques such as discrete fracture network (DFN) or discrete fracture method (DFM) modelling have allowed for efficient simulation of fracture networks; however, variations in permeability are frequently over-simplified (Berre *et al.* 2019). Studies have successfully modelled both end-members of fracture permeability and the integration of fractures within a mesh, separate from the matrix, thus allowing for distinct properties to be applied (e.g. Martin *et al.* 2005; Nordbotten *et al.* 2018). Recent advancements in these methods have enabled the modelling of conduit–barrier systems independently within finite elements (Poulet *et al.* 2021). Applying these approaches to fracture networks and assigning variable permeabilities to the individual fracture generations reduce the uncertainties involved in homogenizing fluid flow through fractured rock.

This contribution primarily focuses on implementing an efficient method for reliable homogenization of fluid flow properties using small-scale fractured outcrop analogues which can be implemented in a large-scale model. The simulations will be analysed based on a regional context assessing how large-scale structures may affect permeability. Improving this type of method is a vital initial step towards developing large-scale models for fractured geothermal systems of low-permeable host rocks (e.g. limestone) where subsurface data may be unavailable or limited and the use of outcrop analogues is essential.

Fig. 1. Tectonic overview of central Germany and the Franconian Basin showing the main fault lines and basins within the region (modified from Peterek *et al.* 1996; Kämmlein *et al.* 2017).

2. Geological setting of the Franconian Basin

2.a. Structural overview of the Franconian Basin

The outcrops analysed in this contribution are located within the Franconian Basin, northern Bavaria (Fig. 1). The Franconian Basin is primarily composed of Late Palaeozoic to Mesozoic sediments with thicknesses up to 3500 m and bounded to the east by the Franconian Lineament and the Bohemian Massif (Schröder, 1987; Peterek *et al.* 1997; Schröder *et al.* 1997). Subsidence and crustal extension related to the culmination of the Varsican Orogeny formed half-graben and graben structures allowing for deposition to occur from the Late Palaeozoic onwards (Freudenberger & Schwerd, 1996; Bauer, 2000; Schäfer *et al.* 2000; Kroner *et al.* 2007). The Franconian Basin deposition spans from Permian (Rotliegend) to Cretaceous and is formed of sandstones, siltstones, mudstones and limestones (Schröder, 1987; Schäfer *et al.* 2000, Freudenberger *et al.* 2013; Kämmlein *et al.* 2017). The outcrops of interest lie within the Malm (Upper Jurassic) limestone unit deposited as an extensive carbonate-dominated platform (Franconian Platform) along the passive Tethyian margin (Meyer & Schmidt-Kaler, 1990; Ziegler 1990; Schintgen & Moeck, 2021).

The basin has experienced several major regional events occurring syn- and post- sedimentation along the pre-existing Varsican structures, commencing with a major compressive phase of deformation that occurred during a Late Cretaceous Inversion causing steep-angled reverse and NW–SE-trending strike-slip faults (e.g. Peterek *et al.* 1993, 1996, 1997; Mazur *et al.* 2005; Kley & Voigt, 2008; Navabpour *et al.* 2017; Voigt *et al.* 2021). Compressional structural features related to this phase are primarily found within the main thrust fault zones whilst the strike-slip components are formed in the areas between faults (Peterek *et al.* 1996).

Following the inversion, the European Cenozoic Rift System initiated an extensional regime, and normal faults and related structural features formed within the basin (Ziegler, 1992; Dèzes *et al.* 2004; Rajchl *et al.* 2009; Voigt *et al.* 2021). This rifting system is found across northern Europe and results in the formation of large NE–SW-striking grabens and half-grabens (Eger Graben; see Fig. 1) east of the Franconian Basin (Schröder, 1987; Peterek *et al.* 1997; Schröder *et al.* 1997; Dèzes *et al.* 2004).

The final phase of major deformation is the Alpine Orogeny during the Eocene convergence of Africa and Europe (e.g. Scheck-Wenderoth *et al.* 2008; Köhler *et al.* 2020). This event caused a large strike-slip regime in the region corresponding to a NW–SE compressional NE–SW extensional stress field (Schröder *et al.* 1997; Wagner *et al.* 1997; Zulauf & Duyster, 1997; Köhler *et al.* 2020). In the Franconian Basin, this phase primarily causes the reactivation of the eastern fault system (Peterek & Schröder, 2010).

The deformation caused by these major phases significantly influences the large-scale faults in the region (Köhler *et al.* 2020). At the site in Kirchleus, the main fault that influences the structural features is the Kulmbach Fault, part of the Franconian Fault System (Heinrichs *et al.* 1994; Peterek *et al.* 1996). This fault is located *c.* 30 m from the quarry (Fig. 2) and records a reverse throw of *c.* 800 m, positioning the Muschelkalk (Trissaic) beside the Malm units (Behrens *et al.* 1967; Franke, 1989; Fazlikhani *et al.* 2022).

2.b. Geothermal potential and exploration of the Franconian Basin

Current geothermal exploration of the Franconian Basin suggests the main heat source may be deep-seated late-Varscian granite intrusions within the Saxothurigan crust underlying the sedimentary cover (Kämmlein et al. 2017; de Wall et al. 2019; Drews et al. 2019). This causes a geothermal gradient of 38 °C km^{-1} observed in the Obernsees 1 borehole (Stettner & Salger, 1985; de Wall et al. 2019). Recent studies have primarily focused on characterizing and modelling the deep geothermal potential of the granite systems; however, little research has been undertaken to explore the fractured sedimentary cover and the influence of the fracture networks on geothermal flow (Kämmlein et al. 2017; de Wall et al. 2019; Bohnsack et al. 2020). In the Molasse Basin (Fig. 1) to the south, the Malm unit is currently utilized for geothermal energy where structural features (fractures, faults and karst) play a key role in producing high flow rates up to 10^{-4} m s^{-1} to the north of the basin (Birner et al. 2012; Birner, 2013; Przybycin et al. 2017; Bohnsack et al. 2020; Schintgen & Moeck, 2021). It is therefore important that geothermal flow through fractured networks of the Franconian Basin be better understood for future exploration.

3. Structural analysis of outcrop analogue

3.a. Analysis of Kirchleus Quarry

Kirchleus Quarry (4×10^4 km^2) is located on the western flank of the Franconian Basin (Fig. 1) within the Malm Formation and in the footwall of the Kulmbach Fault situated 7 km SW of the Franconian Lineament. The quarry complex (Fig. 2) is split into two areas: towards the north, an inactive quarry site contains c. 14 fractured quarry cliff sections (outcrops 1 and 2); towards the south, active quarrying is still operating where the most recently exposed cliff sections are located (outcrop 3). Both sites provide good access, making it possible to measure features within the fractured outcrops and to take detailed images for structural analysis.

These fractures, faults and other structural features can be divided into several stress fields through cross-cutting relationships. The oldest observed structural lineations are observed through normal faults trending NW–SE, with associated striations indicating a NE–SW extension (Fig. 3a).

Reverse faults orientated 025/59 and 200/50 (azimuth/dip) are observed within the quarry and as reactivated structural lineations of the previous extensional features. The movement on these faults and associated tectonic stylolites (σ1 ~ 205°) corresponds to NE–SW compression (Fig. 3b). Strike-slip faults (Fig. 3d) orientated 244/80 and 131/85 are observed to cross-cut these previous structural features and record a NNE compression. Also observed within this set of faults are reverse oblique faults (Fig. 3c) orientated 225/43, recording a similar NE–SW-directed compression. These also appear to cross-cut the structural features observed in Fig. 3b, and these three groups of faults and fractures (Fig. 3b–d) appear the most dominant structural features in the quarry.

A set of dextral strike-slip faults orientated 252/82 and 110/85 (Fig. 3e–f) cross-cut the tectonic stylolites from the previous compressional stress field. Furthermore, tectonic stylolites related to these strike-slip faults are present in a NW–SE compressional direction. These structural features represent the youngest faults that outcrop in the quarry sections.

3.b. Analysis of 2D quarry outcrops

To present the capabilities of the modelling process and the impact of the Kulmbach Fault on the fracture network, three 5 m × 5 m fractured outcrops are imaged at increasing distance from the fault (Fig. 2). The outcrops captured the main fractures within the quarry described in Section 3.a which represent the different deformation phases within the Malm unit. In order to analyse networks present, the images are processed, and fractures are traced using a digital graphics editor (Fig. 4). Geometric analysis of the network is undertaken using FracPaQ which provides results of connectivity and density of the fracture traces (Healy et al. 2017).
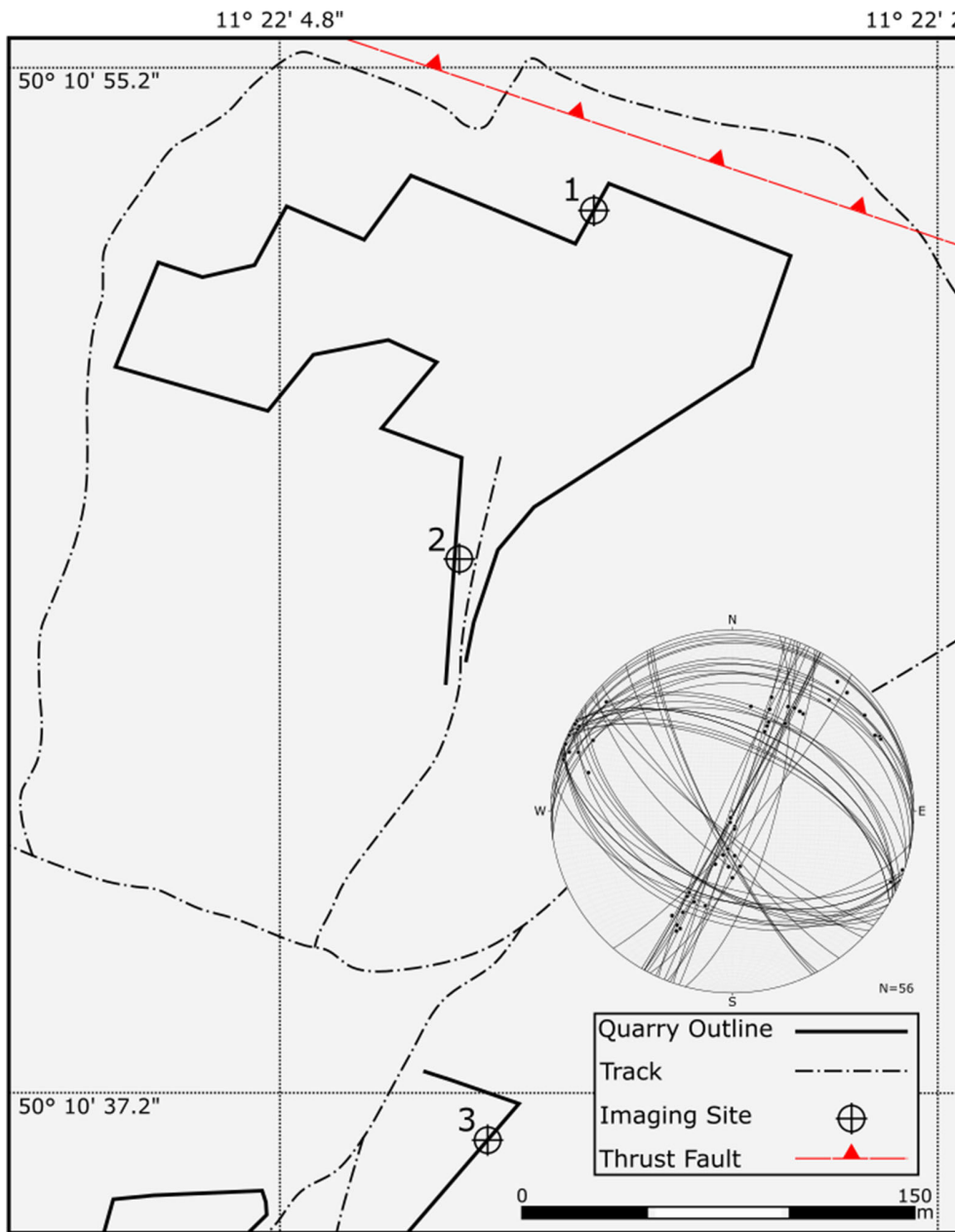
The fractures vary in orientation, spacing and fill. Five different sets are identified (Table 1; Fig. 4) across the three fractured outcrops identified and measured in the field. Fracture set orientation is averaged for each set by calculating the Fisher distribution mean vector (Fisher et al. 1993; Cardozo & Allmendinger, 2013). Not all sets are observed at every outcrop; however, sets 1–3 are consistent throughout. Bedding is represented within set 1 and is treated as structural lineation. This is due to observed structural movements along the bedding planes acting as faults and fractures and therefore these planes can be considered a structural set. The outcrops are all approximately perpendicular to the main Kulmbach Fault to provide a suitable comparison between sites at increasing distance from the fault.

Geometric analysis of the outcrops indicates that whilst average trace length varied between outcrops 3.2 m, 1.86 m, 2.76 m respectively, fracture density (P20) across the 2D traces are similar (5.2 m^{-2}, 5.7 m^{-2}, 4.4 m^{-2}). Connectivity between the nodes of the fracture traces (Table 2) based on Y-X-I analysis (Manzocchi, 2002) shows the fractures are well connected with intersections (X) and relatively few are isolated fractures.

3.c. Integration of geological data into numerical simulations

In order to simulate fluid flow through the fractured outcrops assessed from Kirchleus, several parameters are obtained and estimated from the structural analysis. Based on field observations, the fractures were sorted as open (conduits), closed or filled (barriers) (Fig. 5). As this study focuses primarily on field-based data, the apertures from the field are used for the fluid flow simulations; however, it is known that aperture can vary (increase and decrease) from surface to subsurface due to elevated fluid pressure (e.g. Ghassemi & Kumar, 2007) or in situ stresses (e.g. Bisdom et al. 2016). In order to undertake the fluid flow simulation, a general estimation of aperture and corresponding fracture permeability is required. This is difficult to obtain and for this work we measure aperture for each of the five fracture sets determined from the field through an approximation of fracture widths (Table 1) using image processing software. From these values, permeability along the fracture (longitudinal permeability) is estimated using empirical cubic laws which approximate fracture permeability of each set based on the Hagen–Poiseuille solution of the Navier–Stokes equation (Snow, 1969; Witherspoon et al. 1980; Zhang, 2019). These values indicate that flow could more likely occur through sets 3 and 4 compared to set 1 which is infilled. The values are used as the initial input for the numerical modelling of the sets to simulate the flow through the network.

In addition to the estimated permeability values, the digitized cliff sections provide the base for a discrete fracture network from which a fractured mesh can be generated for numerical simulations. The fractured mesh is used in combination with the different

Fig. 2. Sketch outline of Kirchleus Quarry showing the locations of the studied fractured cliff sections for numerical modelling. Stereonet shows the main fracture orientations observed along the outcrops within the quarry.

fracture permeabilities for each set as the initial input for the numerical modelling. This process presents a method that utilizes fractured outcrop analogue structural data in the homogenization and simulation of fractured networks.

4. Fractured numerical modelling

4.a. Numerical homogenization of the permeability tensor

Instead of simply using only empirical laws with the property of the fracture network, a more exact determination of the full permeability tensor can be obtained through a homogenization procedure based on numerical fluid flow simulations through the fracture network. The permeability K can be expressed in its tensorial form from Darcy's law:

$$\begin{pmatrix} v_x \\ v_y \\ v_z \end{pmatrix} = \frac{1}{\mu_{\mathrm{f}}} \begin{pmatrix} K_{xx} & K_{xy} & K_{xz} \\ K_{yx} & K_{yy} & K_{yz} \\ K_{zx} & K_{zy} & K_{zz} \end{pmatrix} \begin{pmatrix} \nabla P_x \\ \nabla P_y \\ \nabla P_z \end{pmatrix} \qquad (1)$$

where v_i denotes the flow velocity, μ_{f} the fluid viscosity, and ∇P_i the pressure gradient.

In order to isolate any specific component of the permeability tensor K_{ij}, Eq. (1) shows that we can constrain the fluid flow to a single direction j such that the resulting pressure gradient vector is equal to $\nabla P_j = \Delta P_j / L_{j,\mathrm{ref}}$, where $L_{j,\mathrm{ref}}$ represents the reference length of the model in that direction and ΔP_j is the corresponding pressure differential between the boundaries. In this case, we can extract K_{ij} from Eq. (1), expressed as:
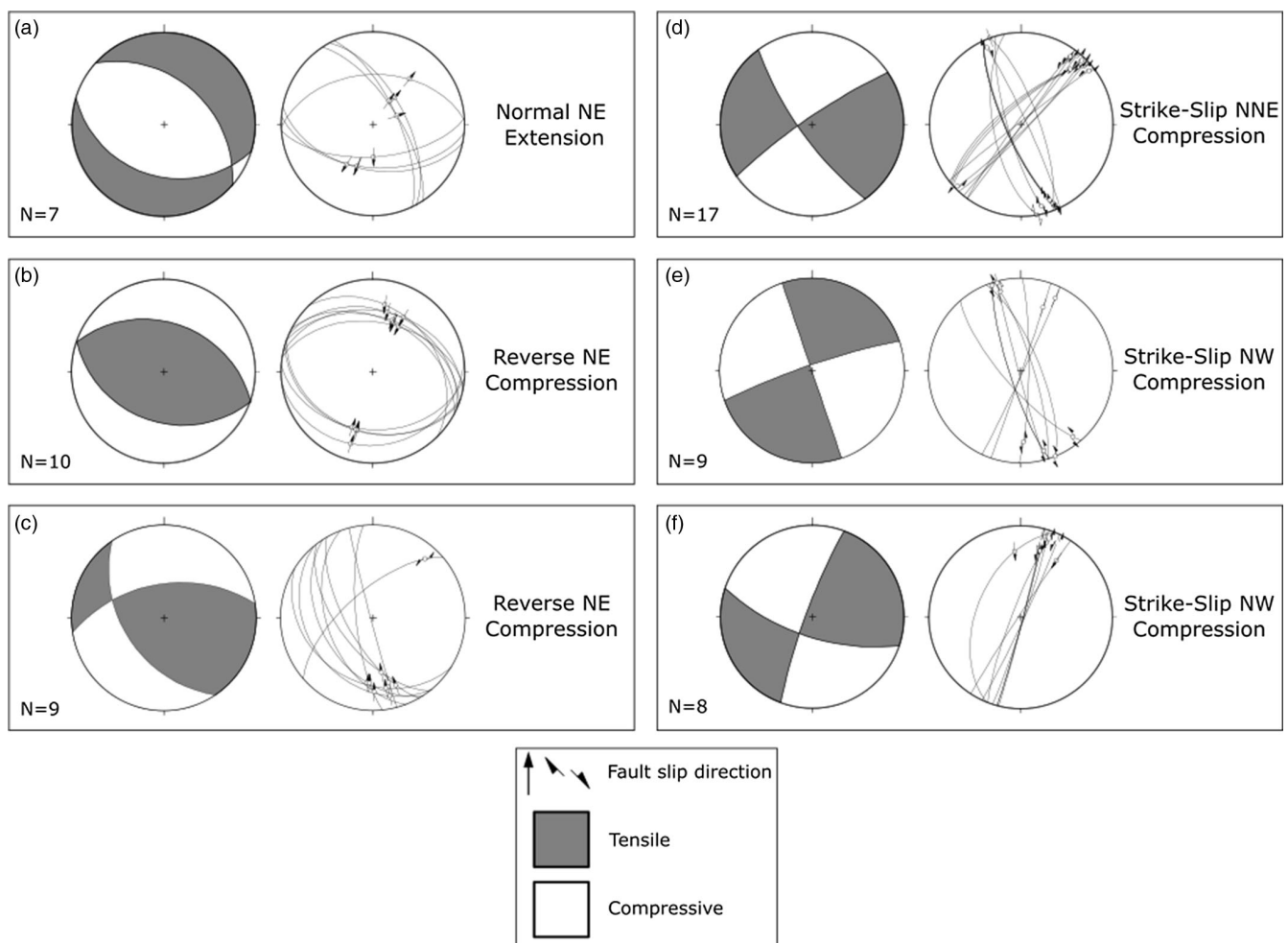
Fig. 3. Fracture results and interpreted stress fields from Kirchleus Quarry showing the main deformation phases affecting the Malm at the outcrop (Köhler et al., 2022).
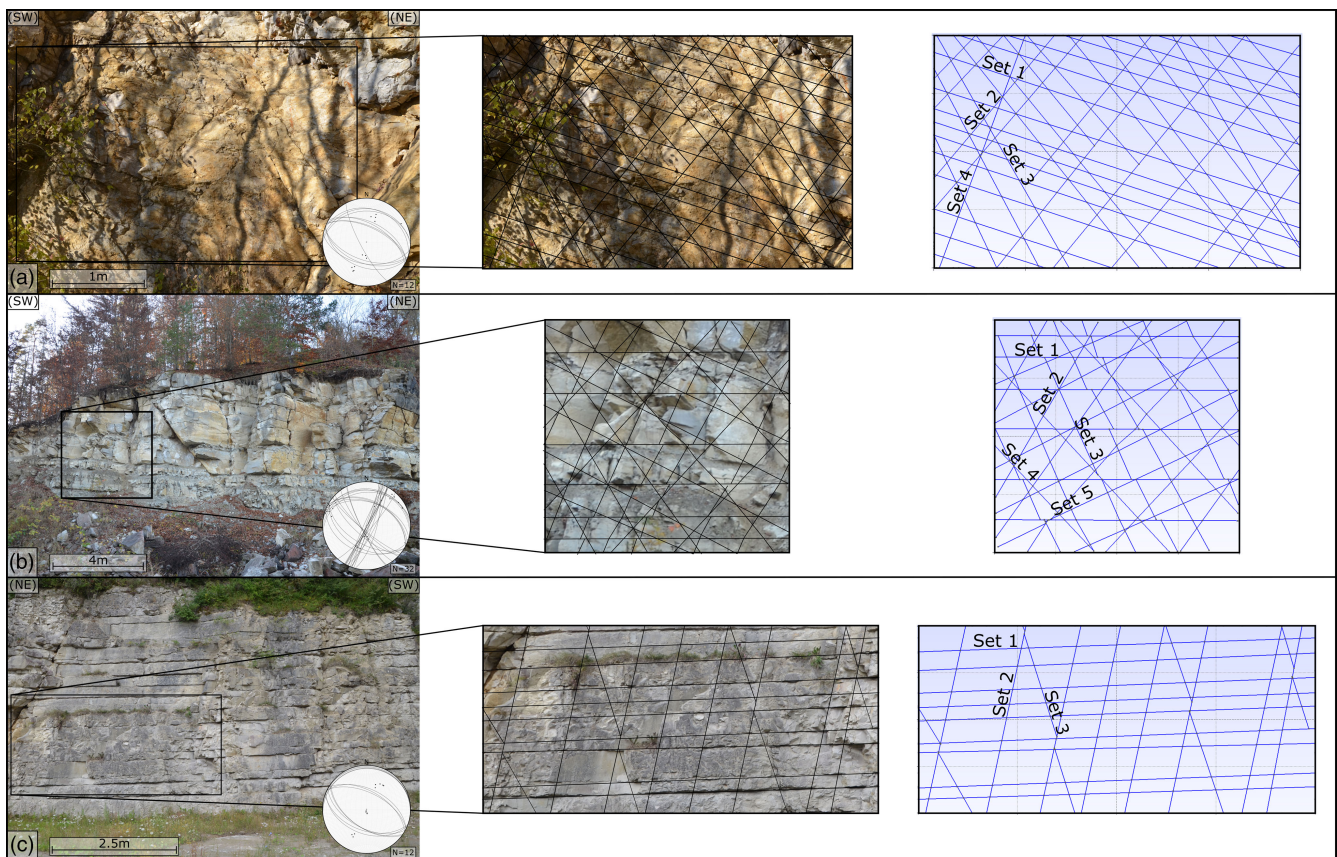
$$K_{ij} = \frac{\mu_f L_{j,\text{ref}} v_i}{\Delta P_j}, \quad 1 \leq i \leq 3 \tag{2}$$

To obtain every component of the permeability tensor, three simulations need to be run, each with a pressure gradient imposed in one different orthogonal direction, from which the longitudinal and transversal fluid velocity can be post-processed. Note that experimental methods cannot calculate the off-diagonal components of the permeability tensor because, as seen from Eq. (4) further below, velocities transversal to the direction of the flow need to be measured, which is very complex to do (Renard *et al.* 2001). This numerical method is therefore the only way to obtain the full permeability tensor. At the scale of fracture networks, fluid flow is already described by Darcy's law, with the rock matrix usually having a different permeability than the fractures. The simulations performed for homogenizing the permeability tensor then consist in solving for Darcy's law through the matrix and the fracture network as explained in the following subsections for a fluid flow in one given orthogonal direction, then post-processing for the value of the fluid velocity.

To homogenize the network, the flow is simulated with the finite element method. Several FEM solvers are available to run numerical simulations of fluid flow through fractured media, including ABAQUS (e.g. Cruz *et al.* 2019), COMSOL Multiphysics (e.g. Koyama *et al.* 2009; Lepillier *et al.* 2019) and

MOOSE Framework (e.g. Grimm Lima *et al.* 2020; Poulet *et al.* 2021), and various methods have been developed through these solvers (Berre *et al.* 2019). We use the open-source finite element simulator REDBACK (Poulet *et al.* 2017) based on the Multi-physics Object Oriented Simulation Environment (MOOSE; Permann *et al.* 2020). The applied REDBACK functionalities have been developed directly for fault-reactivation simulations (e.g. Lesueur et al. 2020; Poulet *et al.* 2021), and MOOSE provides adaptability of the solver for new development and in modifying existing meshes generated initially in GMSH (Geuzaine & Remacle, 2009).

The simulations require a finite element mesh of the 2D fracture features captured from Kirchleus Quarry as discrete fracture networks (DFN; Fig. 4). The use of the DFN is necessary for the simulations as the individual fractures are required to be treated as infinitely thin geometric features (lower-dimensional elements) whereby their thickness is implemented within the flow equations. By using the fracture networks as lower-dimensional elements within the mesh in which the fractures defined in the DFN are treated as an interface between lower-dimensional elements, the complexities involved can be reduced and the process becomes more efficient compared to continuum-based methods (Cacace & Jacquey 2017; Poulet *et al.* 2021). This process removes the necessity for very small elements within the discretized fracture and reduces the elements within the mesh.

Fig. 4. Fractured cliff sections and digitized interpreted fracture traces from Kirchleus Quarry. Sets identified in fracture traces correspond to the sets presented in Table 1.

4.c. Outcrop to 2D fractured mesh

A script has been developed to create the 2D fractured mesh from the traced networks (SVG) using GMSH (Geuzaine & Remacle, 2009) which independently meshes the network of fractures from the matrix. The script identifies the intersection and end nodes of each fracture and converts these into points and lines within GMSH. This provides additional control on the handling of specific nodes, in particular for nearby nodes that should be merged. The geometries are assigned as physical lines within separate groups/sets based on the orientation of the fractures. This tagging process through GMSH allows the fractures to be used in the 2D fluid flow modelling as lower-dimensional elements. This enables the engine to focus the modelling on the fractures independently of the matrix and, when grouping the fractures by orientation, variation of property values can be implemented. To allow the setting of periodic boundary conditions at the numerical stage, extra nodes are also inserted on the bounding box (lines) to ensure that all boundary nodes match on the opposite faces.

4.d. DFN simulation and post-processing

With the mesh generated, finite element simulations can be run to solve for Darcy's law and the fluid mass balance described in steady state as a diffusion of pressure:

$$\nabla \cdot \nabla P = 0 \qquad (3)$$

This equation describes the behaviour within the rock matrix. The DFN is treated separately. The fractures are modelled as lower-dimensional interfaces (Poulet *et al.* 2021) allowing simulation of any kind of behaviour for the fracture, from conduit to barrier, and distinguishing longitudinal flow from transversal, allowing for the implementation of more complex conduit–barrier type of behaviour. The system requires as input the aperture (0.1 cm), as well as the longitudinal and the transversal permeability values associated with each fracture. Two simulations are run for each site: (1) fully homogeneous case where all fractures are of equal permeability (transversal = 0.01 mD; longitudinal = 100 mD); (2) non-homogeneous case where longitudinal permeability of each fracture is controlled by orientation (Table 1). This range of permeability values is justified from the measured aperture and previous fault permeability modelling (Cappa & Rutqvist, 2011).

For the simulation set-up, the pressure gradient is imposed through a high-pressure value as Dirichlet boundary condition at the inlet and a low value at the outlet. On the other sides, periodic boundary conditions of pressure are imposed between parallel faces. Results of the simulations for site 1 of DFN can be seen in Fig. 6.

In order to solve for Eq. (2), the average value of the fluid velocity needs to be computed, where the challenge is to correctly take into account the contribution of the DFN. Specifically, fluid velocity is integrated over the whole domain but the integral over the DFN has to be multiplied by the virtual aperture *a* to consider the correct volumetric contribution of the fractures. Similarly, the virtual volume of the fractures needs to be added to the total volume for the averaging. The average of fluid velocity in one direction is eventually post-processed as:

Table 1. Structural parameters of the measured fracture sets observed and estimated within the fractured outcrops

Set	Site	Average orientation	Conduit or barrier	Estimated aperture (mm)	Longitudinal permeability (mD)
1	1,2,3	004/17	Barrier (clay infill)	0.05	1.00E+01
2	1,2,3	204/50	Semi-conduit	0.175	4.00E +02
3	1,2,3	025/52	Conduit	0.25	1.00E+03
4	1.2	232/79	Conduit	0.25	1.00E+03
5	2	116/83	Semi-conduit	0.15	2.50E+02

Table 2. Y-X-I connectivity of the fractured outcrops

	Y-X-I connectivity (%)			
Site	Y (abutment)	X (intersection)	I (isolated)	Total Points
1	0.01	0.84	0.15	1084
2	0.07	0.68	0.24	1132
3	0.01	0.79	0.20	520

$$\overline{v}_i = \frac{1}{V^M + a \times A^F}\left(\int_M v_i^M + a\int_F v_i^{F,l} + a\int_F v_i^{F,t}\right) \quad (4)$$

where V^M is the total volume of the matrix, A^F the area of the fracture network, v^M the fluid velocity in the matrix, $v_i^{F,l}$ the fluid velocity longitudinal to the fractures and $v_i^{F,t}$ the fluid velocity transversal to the fractures.

4.e. Permeability ellipses

The raw permeability tensors (Table 3) do not allow the properties of the fracture network to be read directly. Instead, most geoscientists prefer to plot ellipses associated with the symmetrical part of the tensor. The ellipses can be plotted using the eigenvalues of the tensor for the radii, and the orientation of the eigenvectors for the rotation of the ellipse. From this plot (Fig. 7), one can visually assess θ, the direction of the principal axis of flow, K_{max}, the maximum value of permeability found on the principal axis, and K_{min} the minimum value.

The permeability ellipses show that the highest K_{max} for both scenarios is from site 1, closest to the main Kulmbach Fault, whilst the lowest K_{max} is within site 3. The lowest K_{min} is also located at site 1. For both sites 1 and 2 the ellipse from the non-homogeneous case, whereby the fracture permeability is defined by variation in orientation, is larger than the ellipse for the homogeneous case. At site 3, the non-homogeneous case is more spherical and has a lower K_{max} than the corresponding homogeneous case. In general, this points towards the non-homogeneous case showing a higher permeability than the homogeneous case. Site 1 also shows strongly orientated ellipses with θ orientated −29.0° and −42.5° respectively for each scenario, whilst the ellipses for sites 2 and 3 show a more level and spherical shape.

The results of the numerical modelling show the capability of using fault and fracture information from outcrop images to simulate fluid flow through the networks to homogenize and extract permeability tensors which can be used for upscaling to geothermal reservoir scale.
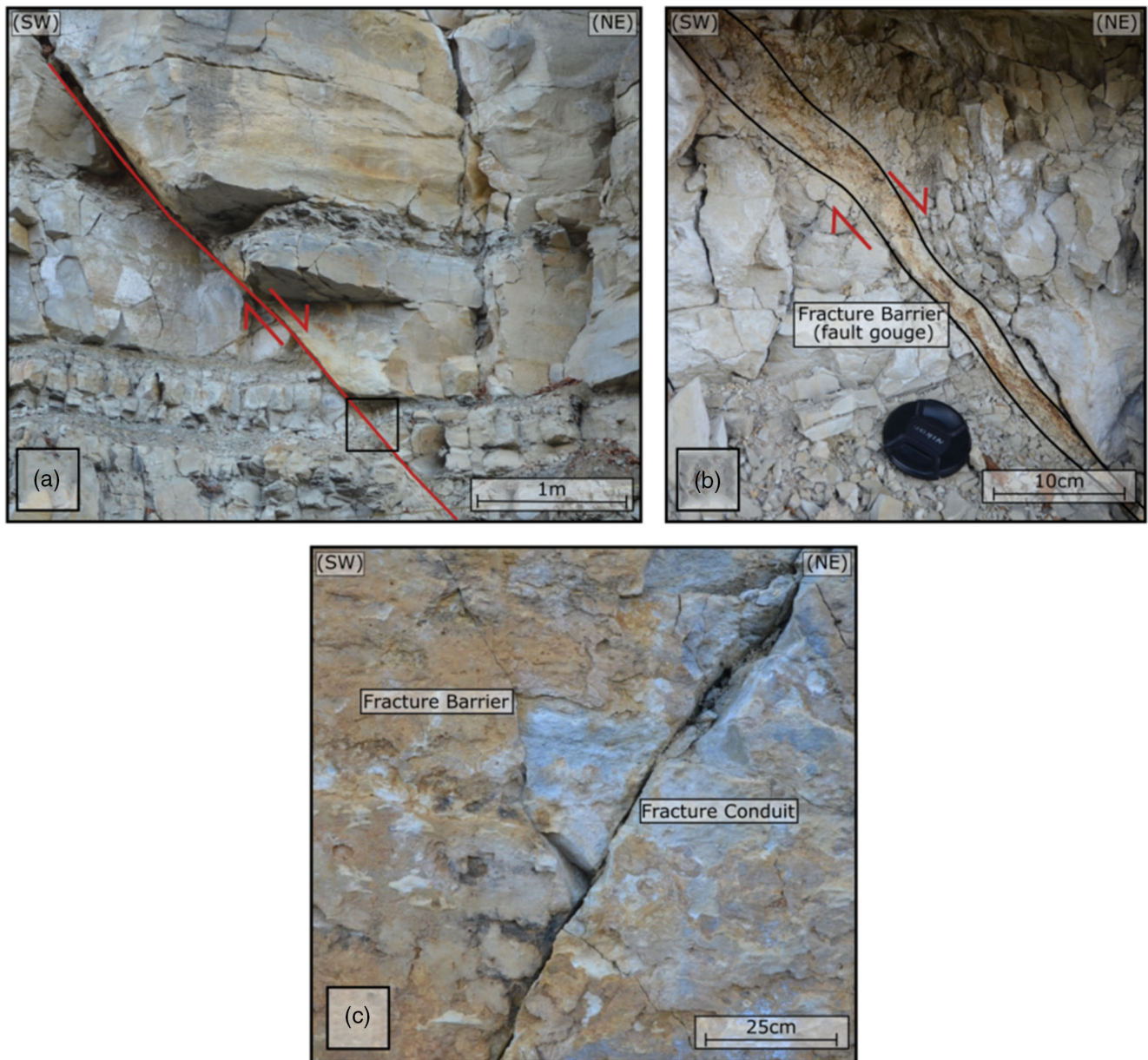
5. Discussion

The results of the structural analysis and numerical simulations show how outcrop analogues can be used to model fluid flow and the effect of varying permeabilities of the fracture sets on fluid transport. Furthermore, this process can act as initial steps towards upscaling and larger-scale numerical simulations of geothermal fluid flow for the Northern Bavarian region, and in particular the use of faults and fractures as flow medium.

5.a. Effect of variable fracture permeability on fluid transport

The permeability tensors and associated ellipses (Fig. 7) presented in the results show that during homogenization varying permeability values of the fractures could have a large impact on the flow magnitude and orientation. For sites 1 and 2, the permeability ellipses for a constant permeability across all fractures (Fig. 7, black ellipses) are smaller than when the permeability is controlled by fracture orientation (Fig. 7, red ellipses). For site 3, it is shown that the ellipses controlled by fracture orientation have a lower K_{max} (0.93D) compared to the tensor with constant fracture permeabilities ($K_{max} = 1.07D$). To illustrate the effects of varying fracture permeability, we used the tensors from site 1 to simulate transport of a non-reactive tracer through a 5 m × 5 m block (Fig. 8). This allows for transport through a homogenized area using the obtained tensor values to be simulated. The simulation was performed with a constant time increment (1 hour) for 48 hours and with a constant pressure gradient from right (5E5 Pa) to left (1E5 Pa) with a normalized constant tracer concentration of 1 at the source node.

The results of the simulation show that there is a significant difference in tracer concentration (Fig. 8c) between the two simulations such that treating the fractures with varying permeabilities influences the transport orientation compared to fractures with a constant permeability value. Furthermore, given that the differences observed in this simulation over a 5 m × 5 m block are significant, the results over a larger area, for example at reservoir scale (kilometres), would be even more pronounced. Therefore, the data suggest that the homogenization of the fracture network is unlikely to result in a realistic scenario for fluid flow simulations. This highlights the importance of defining the fracture apertures and permeabilities prior to numerical simulations during the homogenization process and understanding the effects of upscaling the fracture networks to larger areas and volumes.

The fracture networks simulated within this contribution are treated as linear lower-dimensional elements with assigned permeability values across the interface. Previous fracture studies have also shown that other fracture properties can influence the fluid flow within the network. Properties such as fracture roughness and tortuosity have been modelled to show the impact on flow from including channelling which reduces the efficiency of the network (Li *et al.* 2016; Liu *et al.* 2016; Lee & Babadagli, 2021). Whilst this property is an important feature in fracture flow simulations, as the networks in this study treat the fractures as lower-dimensional elements within the mesh, the effects of other fracture properties can be accounted for numerically (Cacace & Jacquey 2017; Poulet *et al.* 2021). As this method treats the fracture as a flat interface between lower-dimensional elements, the properties (e.g.

Fig. 5. Fracture aperture variation observed at Kirchleus Quarry. (a) Normal fault within the Malm unit observed at site 2 (Fig. 2). (b) Clay infill of the normal fault (Fig. 5a) showing evidence of a fracture barrier to flow. (c) Fractures observed at site 1 showing examples of open and closed sets of fractures which act as conduits and barriers to flow respectively.

aperture and roughness) are accommodated numerically, creating a more efficient simulation.

The numerical methodology presented in this contribution shows a process that can effectively homogenize fracture networks and reduce uncertainties occurring during the upscaling process that can have significant impacts on fluid transport. In terms of geothermal energy, understanding where the tracer is transported to is vital for development planning to create an efficient geothermal system and avoid contamination of the surrounding area.

5.b. Influence of regional events and seismic structures

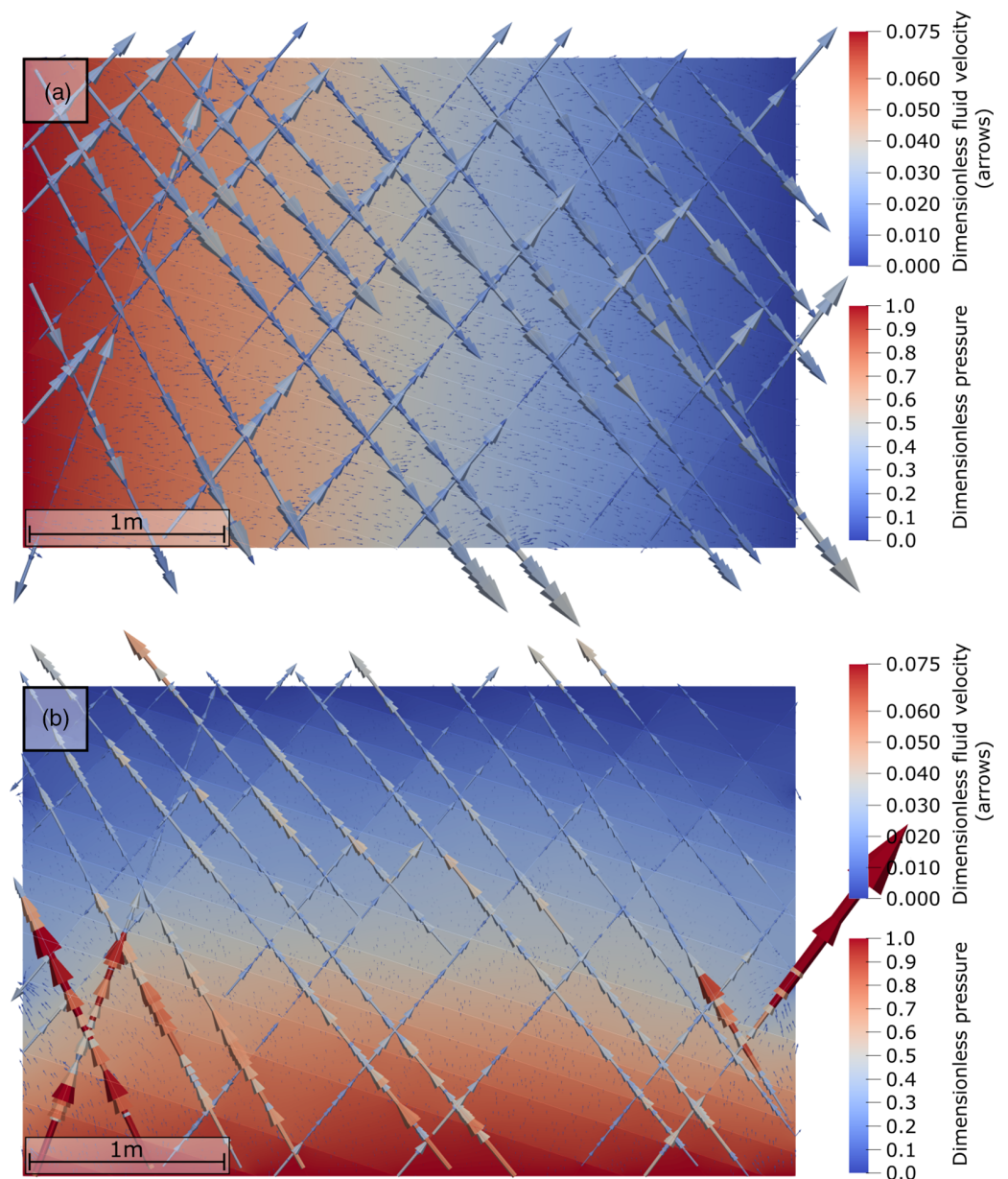### 5.b.1. Regional stress fields from outcrop analysis

The structural features observed in the quarry outcrops (Fig. 3) present several different deformation phases that have affected the units present. The first phase recorded in the Malm unit of the Franconian Basin is the NE–SW extensional phase (Fig. 3a) which causes normal faulting observed in Kirchleus Quarry. This phase occurred at the earliest Late Jurassic, post-Malm sedimentation and into the Early Cretaceous (S Köhler *et al.*, 2022. Similar structures have been observed in surrounding basins (e.g. Thuringian Basin) and can be related to the continued subsidence in the Central European Basin System throughout the Mesozoic (Scheck-Wenderoth *et al.* 2008; Sollhofen *et al.* 2008; Navabpour *et al.* 2017; S Köhler *et al.*, 2022).

The second stress regime interpreted in the quarry presents a general compressional phase orientated NE–SW (Fig. 3b–d). The structures observed in the outcrops at Kirchleus are related to the Late Cretaceous Inversion deformation phase which involved the uplift and exhumation of the Mesozoic basins (Mazur *et al.* 2005;

Table 3. Calculated permeability tensors for both scenarios at each site from the numerical modelling and homogenization
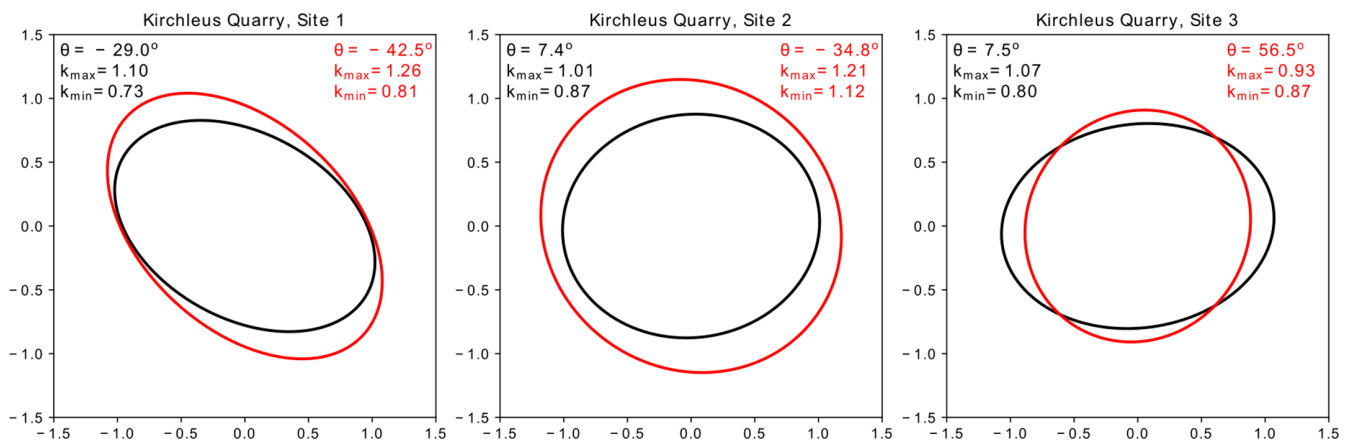
Site	1	2	3
Homogeneous	[1.0127 −0.1529]	[1.0092 0.0173]	[1.0710 0.0246]
	[−0.1592 0.8101]	[0.0175 0.8764]	[0.0361 0.8015]
Non-homogeneous	[1.0608 −0.2200]	[1.1783 −0.0440]	[0.8859 0.0266]
	[−0.2306 1.0109]	[−0.0419 1.1488]	[0.0275 0.9078]

Fig. 6. Pressure distributions and fluid flow velocity vectors of two simulations run with (a) horizontal and (b) vertical pressure gradient on the DFN of cliff section 1 (Fig. 4a).
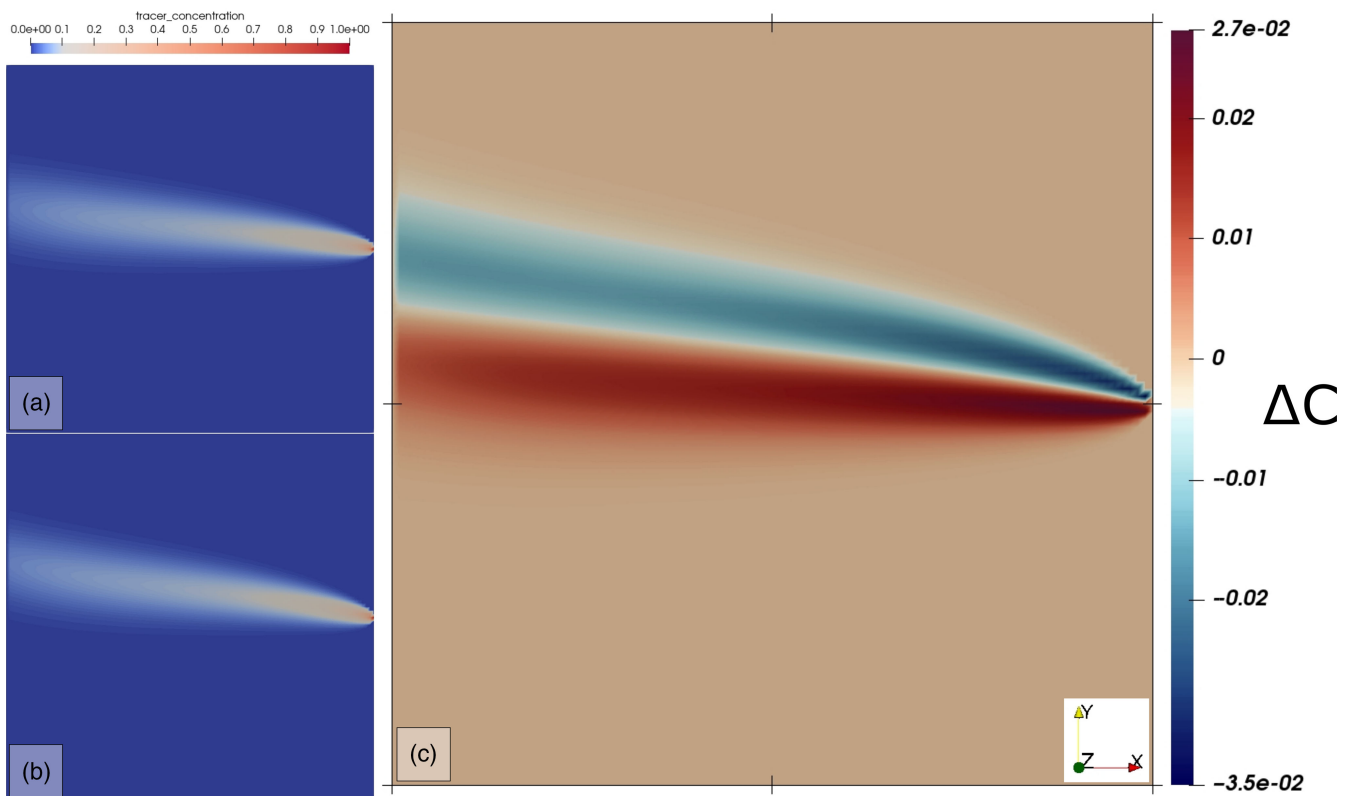
Kley and Voigt, 2008; Voigt *et al.* 2021; S Köhler *et al.*, 2022. It is observed in Kirchleus that this is a multiphase event whereby the initial deformation is primarily composed of the reactivated reverse faults (Fig. 3b) and its culmination characterized by strike-slip faults (Fig. 3d). Furthermore, it is observed that an intermediary transitional phase occurs during the inversion event which forms the oblique reverse faults (Fig. 3c) within the quarry, possibly due to local stress variations and disturbances (Kley and Voigt, 2008;

Sippel *et al.* 2010; Navabpour *et al.* 2017; S Köhler *et al.*, 2022. The reactivation of faults during this phase likely also affected the nearby Kulmbach Fault which influenced the deformation observed in the outcrops, and it is generally observed that inversion deformation causes the largest faults and fractures, controlling the structure of the quarry outcrops observed from satellite view (Fig. 2).

The final stress recorded in Kirchleus Quarry formed the strike-slip faulting (Fig. 3e, f) and tectonic stylolites which overprint the

Fig. 7. Permeability ellipses from the homogenization process and tensor calculation. Black permeability ellipse is calculated using a constant permeability for all fractures. Red permeability ellipse is calculated using varying permeabilities based on fracture orientation. Site 1 shows tilting of the ellipse towards the main Kulmbach Fault. Sites 2 and 3 show lessening impact of the fault to the ellipse orientation and magnitude.

Fig. 8. (a, b) Tracer transport through a 5 m × 5 m block using (a) constant permeability for all fractures and (b) variable permeability controlled by fracture orientation and defined conduit, barrier and conduit–barrier sets. (c) Difference in tracer concentration between the two scenarios. Simulations were performed using the PorousFlow module (Permann *et al.* 2020; Wilkins *et al.* 2021) within MOOSE.

structural lineations formed during the Late Cretaceous Inversion. This NW–SE shortening and thrusting is likely related to the Alpine Orogeny and the regional-scale strike-slip regime affecting Central Europe (Schröder *et al.* 1997; Zulauf & Duyster, 1997; Peterek & Schröder, 2010). These are the youngest natural faults observed within the quarry that are cutting all the other faults.

5.b.2. Influence of the Kulmbach Fault

The importance of faults to fluid flow is well documented through reservoir characterization and development (Caine *et al.* 1996;

Bense *et al.* 2013; Vidal *et al.* 2017; La Bruna *et al.* 2021; Smeraglia *et al.* 2021), and whilst faults can be observed using sub-surface data analysis (e.g. seismic imaging) the fractures related to the faults commonly are not. Therefore, utilizing alternative data sources, such as outcrop analogues, for further understanding the influence of seismic-scale faults on the fracture network and ultimately the fluid flow is vital. Initial results of the structural analysis show that the fractures are well connected and therefore could provide suitable pathways due to the high concentration of fracture intersections. In combination with the results of the numerical

simulations they provide a detailed analysis of the impact of the fault on the fracture permeability.

The Kulmbach Fault is a seismic-scale fault, and the fractured cliff sections analysed were an increasing distance from the fault (Fig. 2). Whilst the results of the permeability tensors and ellipses obtained from homogenization of the fractured outcrops showed the importance of classifying fractures through aperture and permeability magnitude, they also show variation in the ellipses by site. In particular, the influence of the fault on the orientation of the flow patterns is clearly seen. The permeability ellipses for site 1 show a tilted nature (−29.0°) in comparison to the generally horizontal nature of the tensors from site 2 (7.4°) and site 3 (7.5°). The increased dip in the anisotropic permeability is noted as also parallel to the main dip of the Kulmbach Fault. Therefore, the fault directly influences the orientation of the permeability tensors and ellipses and thus fluid flow. Fluid flow orientation is important within the reservoir, particularly when primary permeability is controlled by structural features rather than sedimentological properties as observed within the Malm (Birner *et al.* 2012; Schintgen and Moeck 2021).

However, all the fracture outcrops analysed, and modelled from, have generally the same orientation (NE–SW). Therefore, only the fracture network perpendicular to the fault strike is observed in the results. Whilst this could limit the understanding of the fracture flow parallel to the fault, observing perpendicular fracture networks ensures that the horizontal flow and possible fluid pathways away from the fault are captured.

Furthermore, the magnitude (k_{max}) is also larger at site 1 (1.26D) compared to sites 2 and 3 (1.21D and 0.93D respectively). This implies that the permeability increases towards the fault and thus fluid flow transport could be higher. This increased permeability corresponds to a damage zone near the Kulmbach Fault (Fig. 9). This damage zone is situated on the footwall of the reverse fault and impacts on the fracture networks as seen at site 1. Given that site 1 is located *c.* 30 m from the fault, the damage zone could be up to 100 m from the fault. This large distance could significantly influence the fluid flow around the faults at depth. From the hanging wall towards the ENE another damage zone is expected; however, width is unknown and there are likely additional effects to the fracture networks from the fold–thrust system (e.g. Watkins *et al.* 2018).

Overall, the Kulmbach Fault has a direct influence over fluid transport through the fractured networks. This is important for modelling fractured reservoirs in general, in particular the low-permeability Malm reservoirs, as by further understanding how the faults affect the fracture networks, uncertainties through modelling these faulted systems can be reduced. The outcrop to tensor methodology presented in this paper can be utilized to effectively model, homogenize and upscale these systems, with particular detail on the influence of seismic-scale faults such as the Kulmbach Fault on reservoir flow.

Field-based studies on fracture networks can lead to some uncertainties in the data collection which can be accounted for (e.g. Peacock *et al.* 2019). Outcrop quality is an important factor to consider when capturing 2D imagery of fracture networks, and it is key that a link to the subsurface is established (Gutmanis *et al.* 2018). Kirchleus Quarry was chosen as a suitable site to assess the fractures within the Malm unit of the Franconian Basin due to its close proximity to the main Kulmbach Fault. The quarry provides excellent access to large cliff sections, some of which have limited weathering effects and therefore good outcrops for analysis. However, this could lead to uncertainties and bias from outcrop quality and choice. For fracture network imaging, unweathered, clean outcrops are most effective for tracing lineations for analysis, and therefore these outcrops are preferred over weathered cliff sections. These sections are therefore discounted from analysis and thus fractures may be missed.
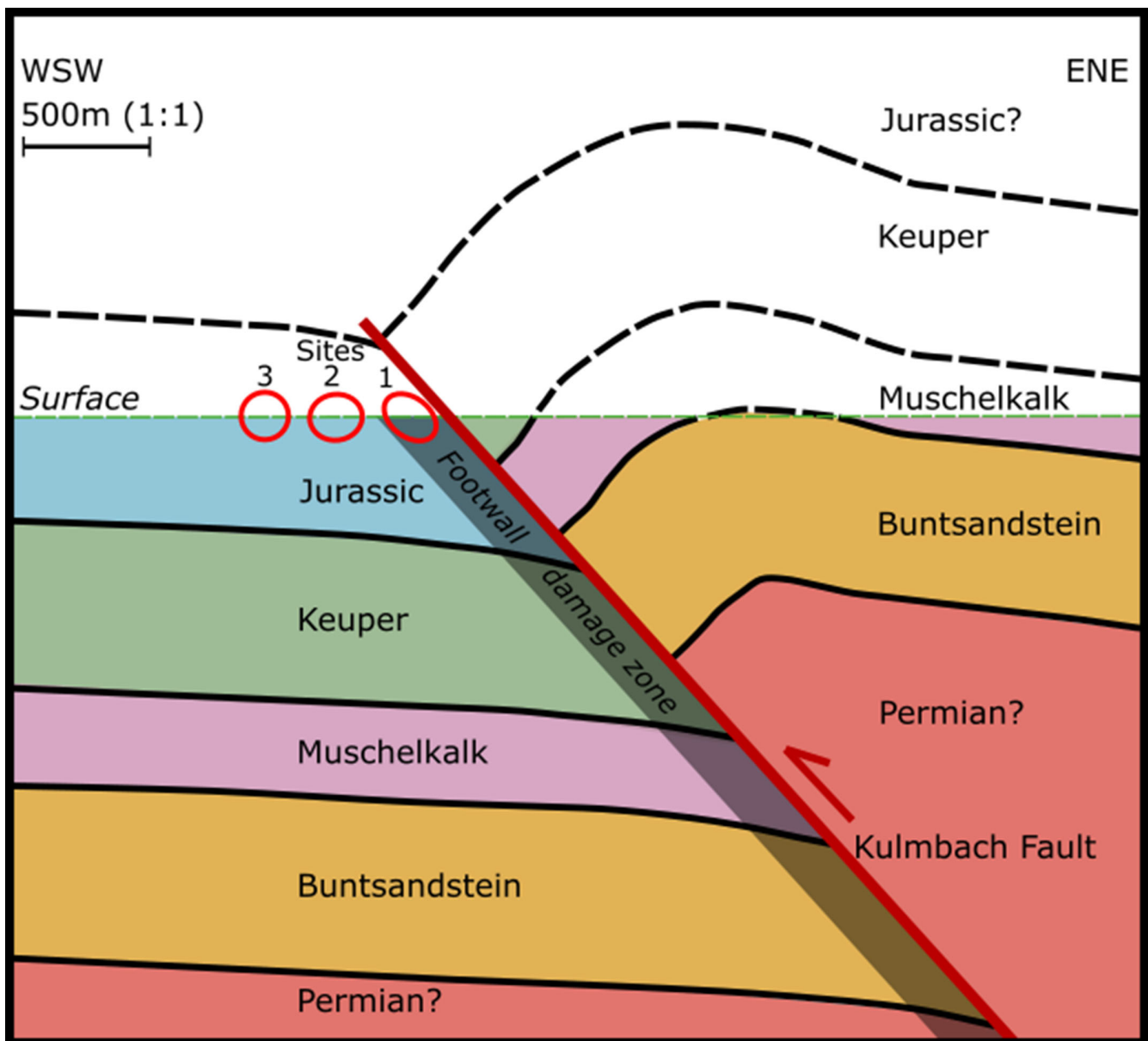
A further consideration when using the fractured analogues is to ensure the captured fractured networks are representative of the modelled network scale. The 5 m × 5 m window size for sampling the fracture networks allows for a large area of the network to be imaged, reducing the sensitivity to bias (Zeeb *et al.* 2013). There are several other methods that could be utilized to estimate the representative scale required for the model, such as Monte Carlo simulations (e.g. Rong *et al.* 2013). However, for the scope of this study we assumed the simulated area is representative of the fracture network observed in outcrop (e.g. Bear, 1972; Bear & Bachmat, 1990; Andrianov & Nick, 2019) and at outcrop scale (up to tens of metres) the imaged networks are suitable for numerical modelling without over- or undersaturation of fractures (Fourno *et al.* 2013; Meier *et al.* 2018; Berre *et al.* 2019; Poulet *et al.* 2021). Furthermore, the selection of the outcrops at increasing distance from the main Kulmbach Fault enables a good spread of data to be collected to minimize fractures lost to bias or outcrop quality, thereby limiting the uncertainties that could arise from the data collection and analysis.

5.c. Implications for the Geothermal system and future modelling

Geothermal energy use is increasingly prevalent, and it is a vital necessity to effectively model these systems and reduce uncertainties in reservoir modelling (Witter *et al.* 2019). Where data for the exploration and development of geothermal projects are limited, analogues can be a useful tool. In the Franconian Basin, there are limited subsurface data and therefore the modelling of the subsurface is driven by outcrop analysis. Work has primarily focused on the geothermal potential of the deep granite systems within the Franconian Basin, with limited emphasis on the influence of structural elements (Kämmlein *et al.* 2017). However, it is known that fracture networks within the Malm in southern Germany (Molasse Basin) contribute significantly to flow (Birner *et al.* 2012; Schintgen & Moeck, 2021).

Karstification is also observed at the Kirchleus outcrop affecting the Malm units and can be both advantageous and disadvantageous to production from carbonate reservoirs. Karst within reservoirs can enhance fluid flow in the subsurface depending on the size of the feature, but also can cause serious uncertainties and safety issues regarding drilling and production (e.g. Sloan, 2003). In Kirchleus, several different karst features are observed in and around the fault zones. Wormholes and vugs up to *c.* 1.5 m wide are recorded within faults, fractures and along stylolites within the limestone. Whilst karstification is outwith the scope of this contribution, it should be noted for future modelling that it is present within the reservoir units and should be considered as a possible subsurface fluid pathway.

The results of the fracture modelling and numerical simulations show that seismic-scale faults are influencing the fracture networks in the vicinity, forming damage zones which could be pathways for geothermal flow at depth. It is also observed that the Malm reservoir in the Franconian Basin hosts good fracture networks formed through several deformation events (Late Cretaceous Inversion and Alpine phases) and that act as the primary conduits for flow. Given that these faults and fractures are linked to deformation

Fig. 9. Conceptual model showing a cross-section through the Kulmbach Fault and how the homogenized permeability of the fracture networks is affected by the fault within the fault damage zone.

phases, it can be predicted that the same networks are located at depth. Therefore, further modelling of the subsurface can use the presence of major faults as a driver for the fracture networks present. The homogenized models presented show the small-scale flow through the Malm units; however, further upscaling (up to km scale) would be required to better model the flow through the reservoir. For this, additional data would be required such as additional larger-scale outcrop sites (e.g. drone imagery) and the use of subsurface data (wells and seismic) to integrate into a reservoir-scale fracture network model.

Currently, new seismic acquisition is underway for northern Bavaria and these additional data could be utilized to directly image the fracture networks at depth to compare with the networks at the surface (Fazlikhani *et al.* 2022). Similar datasets have already been acquired and analysed in the Molasse Basin, and similar approaches and integration from this basin could be utilized within the Franconian Basin (Budach *et al.* 2018; Wawerzinek *et al.* 2021). Seismic in combination with well and outcrop data can be used to create discrete fracture networks (e.g. Smith, 2020; Boersma *et al.* 2021). These DFN models can additionally be driven by the outcrops and the understanding of how the faults are tilting the transport direction, as observed at Kirchleus Quarry. The aperture values used for the numerical modelling were determined directly from outcrop; however, future modelling could integrate the numerical flow simulations with aperture modelling based on current stress conditions at depth (Prabhakaran *et al.* 2018 and references therein). These further fracture acquisition and modelling techniques, in combination with the permeability tensors acquired from outcrop, would enhance understanding of the subsurface structure of the Malm and reduce the uncertainties involved in the geothermal exploration of the Franconian Basin.

6. Conclusions

The Malm units in the Franconian Alps in southern Germany are an important aquifer for geothermal exploration that is dominated by fracture networks which play a vital role in increasing permeability for fluid flow. Structural analysis of the Malm unit within the basin showed that several events have affected the fracture networks present. From the Late Jurassic onwards, an early extensional phase followed by Late Cretaceous Inversion and the Alpine Orogeny have caused movements along major faults (e.g. Kulmbach Fault) which have fractured the limestone formation.

This contribution implements a suitable method for applying 2D outcrop analogue data to the simulation of fluid flow through small-scale fracture networks. The fracture networks have been imaged and digitized to create 2D fracture network models that can be used to analyse and acquire permeability tensors of the Malm units. Analysis of the 2D networks shows that the fractures are well connected through intersections. The networks are meshed and homogenized to acquire the 2D permeability tensors which represent the flow through the rock. The tensors showed that the Kulmbach Fault influences the orientation and magnitude of fluid transport, tilting the flow in the direction of dip. This implies that large-scale (seismic) structures are likely to affect fluid flow in the reservoirs, and, as such, subsurface modelling should account for the effects of these features. There is likely a critical distance at which deformation occurs around the fault. Furthermore, it is shown that variable fracture permeability directly affects the orientation of fluid transport. It is therefore vital for homogenization and upscaling of fracture network flow that conduits, barriers and conduit–barriers are properly quantified. These results of outcrop image to 2D homogenization and permeability tensor acquisition show how using analogues can further improve the understanding of subsurface flow and reduce uncertainty in the modelling of fractured reservoirs.

References

Alboin C, Jaffré J, Roberts JE and Serres C (2002) Modeling fractures as interfaces for flow and transport. In *Fluid Flow and Transport in Porous Media* (eds Z Chen & R Ewing), pp. 13–24. *Mathematical and Numerical Treatment* **295**,. Providence, Rhode Island: American Mathematical Society.

Andrianov N and Nick HM (2019) Modeling of waterflood efficiency using outcrop-based fractured models. *Journal of Petroleum Science and Engineering* **183**, 106350

Araújo RE, La Bruna V, Rustichelli A, Bezerra FH, Xavier MM, Audra P, Barbosa JA and Antonino AC (2021) Structural and sedimentary discontinuities control the generation of karst dissolution cavities in a carbonate sequence, Potiguar Basin, Brazil. *Marine and Petroleum Geology* **123**, 104753.

Bauer H, Schröckenfuchs TC and Decker K (2016) Hydrogeological properties of fault zones in a karstified carbonate aquifer (Northern Calcareous Alps, Austria). *Journal of Hydrogeology* **24**, 1147–70.

Bauer W (2000) Geothermische Verhältnisse des Fränkischen Beckens. *Hydrogeologie und Umwelt* **22**, 1–186.

Bear J (1972) *Dynamics of Fluids in Porous Media*. New York: Elsevier.

Bear J and Bachmat Y (1990) Macroscopic description of transport phenomena in porous media. In *Introduction to Modelling of Transport Phenomena in Porous Media* (eds J Bear and Y Bachmat), pp. 43–262. Dordrecht: Springer.

Behrens M, Jansen A and Wurster P (1967) Untersuchungen an fränkischen Verwerfungen. *Geologische Rundschau* **56**, 748–65.

Bense VF, Gleeson T, Loveless SE, Bour O and Scibek J (2013) Fault zone hydrogeology. *Earth-Science Reviews* **127**, 171–92.

Berkowitz B (1995) Analysis of fracture network connectivity using percolation theory. *Mathematical Geology* **27**, 467–83.

Berre I, Doster F and Keilegavlen E (2019) Flow in fractured porous media: a review of conceptual models and discretization approaches. *Transport in Porous Media* **130**, 215–36.

Birner J (2013) *Hydrogeologisches Modell des Malmaquifers im Süddeutschen Molassebecken*. PhD thesis, Institut für geologische Wissenschaften, Freie Universität Berlin, Berlin, Germany. Published thesis.

Birner J, Fritzer T, Jodocy M, Savvatis A, Schneider M and Stober I (2012) Hydraulische Eigenschaften des Malmaquifers im Sueddeutschen Molassebecken und ihre Bedeutung für die geothermische Erschliessung. *Zeitschrift für Geologische Wissenschaften* **40**, 133–56.

Bisdom K, Bertotti G and Nick HM (2016) The impact of in-situ stress and outcrop-based fracture geometry on hydraulic aperture and upscaled permeability in fractured reservoirs. *Tectonophysics* **690**, 63–75.

Bisdom K, Nick HM and Bertotti G (2017) An integrated workflow for stress and flow modelling using outcrop-derived discrete fracture networks. *Computers and Geosciences* **103**, 21–35.

Boersma Q, Prabhakaran R, Bezerra FH and Bertotti G (2019) Linking natural fractures to karst cave development: a case study combining drone imagery, a natural cave network and numerical modelling. *Petroleum Geoscience* **25**, 454–69.

Boersma QD, Bruna PO, de Hoop S, Vinci F, Tehrani AM and Bertotti G (2021) The impact of natural fractures on heat extraction from tight Triassic sandstones in the West Netherlands Basin: a case study combining well, seismic and numerical data. *Netherlands Journal of Geosciences* **100**, e6.

Bohnsack D, Potten M, Pfrang D, Wolpert P and Zosseder K (2020) Porosity–permeability relationship derived from Upper Jurassic carbonate rock cores to assess the regional hydraulic matrix properties of the Malm reservoir in the South German Molasse Basin. *Geothermal Energy* **8**, 1–47.

Bonnet E, Bour O, Odling NE, Davy P, Main I, Cowie P and Berkowitz B (2001) Scaling of fracture systems in geological media. *Reviews of Geophysics* **39**, 347–83.

Bour O, Davy P, Darcel C and Odling N (2002) A statistical scaling model for fracture network geometry, with validation on a multiscale mapping of a joint network (Hornelen Basin, Norway). *Journal of Geophysical Research: Solid Earth* **107**, ETG 4-1–ETG 4-12.

Bruna PO, Lavenu AP, Matonti C and Bertotti G (2019) Are stylolites fluid-flow efficient features? *Journal of Structural Geology* **125**, 270–7.

Budach I, Moeck I, Lüschen E and Wolfgramm M (2018) Temporal evolution of fault systems in the Upper Jurassic of the Central German Molasse Basin: case study Unterhaching. *International Journal of Earth Sciences* **107**, 635–53.

Cacace M and Jacquey AB (2017) Flexible parallel implicit modelling of coupled thermal–hydraulic–mechanical processes in fractured rocks. *Solid Earth* **8**, 921–41.

Caine JS, Evans JP and Forster CB (1996) Fault zone architecture and permeability structure. *Geology* **24**, 1025–8.

Cappa F and Rutqvist J (2011) Modeling of coupled deformation and permeability evolution during fault reactivation induced by deep underground injection of CO_2. *International Journal of Greenhouse Gas Control* **5**, 336–46.

Cardozo N and Allmendinger RW (2013) Spherical projections with OSXStereonet. *Computers and Geosciences* **51**, 193–205.

Connolly P and Cosgrove J (1999) Prediction of fracture-induced permeability and fluid flow in the crust using experimental stress data. *AAPG Bulletin* **83**, 757–77.

Cox SF (1999) Deformational controls on the dynamics of fluid flow in mesothermal gold systems. In *Fractures, Fluid Flow and Mineralisation* (eds K McCaffrey, L Lonergan and J Wilkinson), pp. 123–39. Geological Society of London, Special Publication no. 155.

Cruz F, Roehl D and do Amaral Vargas Jr E (2019) An XFEM implementation in Abaqus to model intersections between fractures in porous rocks. *Computers and Geotechnics* **112**, 135–46.

Curewitz D and Karson JA (1997) Structural settings of hydrothermal outflow: fracture permeability maintained by fault propagation and interaction. *Journal of Volcanology and Geothermal Research* **79**, 149–68.

de Wall H, Schaarschmidt A, Kämmlein M, Gabriel G, Bestmann M and Scharfenberg L (2019) Subsurface granites in the Franconian Basin as the source of enhanced geothermal gradients: a key study from gravity and thermal modelling of the Bayreuth Granite. *International Journal of Earth Sciences* **108**, 1913–36.

Dershowitz WS and Herda HH (1992) Interpretation of fracture spacing and intensity. In *Proceedings of the 33rd US Symposium on Rock Mechanics, Santa Fe, NM* (eds JR Tillerson and WR Wawersik), pp. 757–66.

Dèzes P, Schmid SM and Ziegler PA (2004) Evolution of the European Cenozoic Rift System: interaction of the Alpine and Pyrenean orogens with their foreland lithosphere. *Tectonophysics* **389**, 1–33.

Drews M, Bauer W, Fazlikhani H, Stollhofen H, Kämmlein M, Potten M, Thuro K and de Wall, H (2019) Ursachenforschung zur geothermischen Anomalie in Nordbayern. *Geothermische Energie* **91**, 10–13.

Elkarmoty M, Tinti F, Kasmaeeyazdi S, Giannino F, Bonduà S and Bruno R (2018) Implementation of a fracture modeling strategy based on Georadar Survey in a large area of Limestone Quarry Bench. *Geosciences* **8**, 481.

Fazlikhani H, Bauer W and Stollhofen H (2022) Variscan structures and their control on latest to post-Variscan basin architecture: insights from the westernmost Bohemian Massif and SE Germany. *Solid Earth Discussions* **13**, 393–416.

Fisher NI, Lewis T and Embleton BJ (1993) *Statistical Analysis of Spherical Data*. Cambridge: Cambridge University Press.

Fourno A, Grenier C, Benabderrahmane A and Delay F (2013) A continuum voxel approach to model flow in 3D fault networks: a new way to obtain up-scaled hydraulic conductivity tensors of grid cells. *Journal of Hydrology* **493**, 68–80.

Franke W (1989) The geological framework of the KTB drill site, Oberpfalz. In *The German Continental Deep Drilling Program (KTB)* (eds R Emmermann and J Wohlenberg), pp. 37–54. Berlin and Heidelberg: Springer.

Freudenberger W, Geyer G and Schröder B (2013) Der Buntsandstein in Bayern (nordwestliches Franken, Bruchschollenland und Randfazies im Untergrund). In *Deutsche Stratigraphische Kommission: Stratigraphie von Deutschland XI. Buntsandstein* (eds J Lepper and HG Röhling), pp. 547–82. Schriftenreihe der Deutschen Gesellschaft für Geowissenschaften. 68. Stuttgart, Germany: Schweizerbart'sche Verlagsbuchhandlung.

Freudenberger W and Schwerd K (1996) *Erläuterungen zur Geologischen Karte von Bayern 1:500000*. Munich, Germany: Bayerisches Geologisches Landesamt. 329 pp.

Geers MG, Kouznetsova VG, Matouš K and Yvonnet J (2017) Homogenization methods and multiscale modeling: nonlinear problems. *Encyclopaedia of Computational Mechanics*, 2nd edn (eds E Stein, R de Borst & TJR Hughes), pp. 1–34. New York: Wiley.

Geuzaine C and Remacle J-F (2009) Gmsh: a 3-D finite element mesh generator with built-in pre- and post-processing facilities. *International Journal for Numerical Methods in Engineering* **79**, 1309–31.

Ghassemi A and Kumar GS (2007) Changes in fracture aperture and fluid pressure due to thermal stress and silica dissolution/precipitation induced by heat extraction from subsurface rocks. *Geothermics* **36**, 115–40.

Giuffrida A, Agosta F, Rustichelli A, Panza E, La Bruna V, Eriksson M, Torrieri S and Giorgioni M (2020) Fracture stratigraphy and DFN modelling of tight carbonates: the case study of the Lower Cretaceous carbonates exposed at the Monte Alpi (Basilicata, Italy). *Marine and Petroleum Geology* **112**, 104045.

Giuffrida A, La Bruna V, Castelluccio P, Panza E, Rustichelli A, Tondi E, Giorgioni M and Agosta F (2019) Fracture simulation parameters of fractured reservoirs: analogy with outcropping carbonates of the Inner Apulian Platform, southern Italy. *Journal of Structural Geology* **123**, 18–41.

Grandjean G and Gourry JC (1996) GPR data processing for 3D fracture mapping in a marble quarry (Thassos, Greece). *Journal of Applied Geophysics* **36**, 19–30.

Grimm Lima MM, Schädle P, Vogler D, Saar MO and Kong XZ (2020) A numerical model for formation dry-out during CO_2 injection in fractured reservoirs using the MOOSE framework: implications for CO_2-based geothermal energy extraction. In Proceedings of the World Geothermal Congress 2020, 26th April–2nd May 2020, Reykjavik, Iceland. https://doi.org/10.3929/ethz-b-000410774

Gutmanis J, i Oró LA, Díez-Canseco D, Chebbihi L, Awdal A and Cook A (2018) Fracture analysis of outcrop analogues to support modelling of the subseismic domain in carbonate reservoirs, south-central Pyrenees. In *Subseismic-Scale Reservoir Deformation* (ed. M Ashton), pp. 139–56. *Geological Society of London, Special Publication* no. 459.

Hardebol NJ and Bertotti G (2013) DigiFract: a software and data model implementation for flexible acquisition and processing of fracture data from outcrops. *Computers and Geosciences* **54**, 326–36.

Healy D, Rizzo RE, Cornwell DG, Farrell NJ, Watkins H, Timms NE, Gomez-Rivas E and Smith M (2017) Fracpaq: a Matlab™ toolbox for the quantification of fracture patterns. *Journal of Structural Geology* **95**, 1–16.

Heinrichs T, Giese P, Bankwitz P and Bankwitz E (1994) Dekorp 3/MVE-90(West): preliminary geological interpretation of a deep near-vertical reflection profile between the Rhenish and the Bohemian Massifs, Germany. *Zeitschrift für geologische Wissenschaften* **22**, 771–801.

Hollinsworth AD, Koehn D, Dempster TJ and Aanyu K (2019) Structural controls on the interaction between basin fluids and a rift flank fault: constraints from the Bwamba Fault, East African Rift. *Journal of Structural Geology* **118**, 236–49.

Howell JA, Martinius AW and Good TR (2014) The application of outcrop analogues in geological modelling: a review, present status and future outlook. In *Sediment-Body Geometry and Heterogeneity: Analogue Studies for Modelling the Subsurface* (eds A Rittersbacher, SJ Buckley, JA Howell, GJ Hampson and J Vallet), pp. 1–25. Geological Society of London, Special Publication no. 387 .

Jaglan H, Qayyum F and Hélène H (2015) Unconventional seismic attributes for fracture characterization. *First Break* **33**, 101–109.

Jones RR, McCaffrey KJW, Clegg P, Wilson RW, Holliman NS, Holdsworth RE, Imber J and Waggott S (2009) Integration of regional to outcrop digital data: 3D visualisation of multi-scale geological models. *Computers and Geosciences* **35**, 4–18.

Kämmlein M, Bauer W and Stollhofen H (2017) New thermophysical data pool for NE-Bavaria reveals exceptionally high local heat fluxes. In German Geothermal Congress (GGC 2017), 12th–14th September 2017, Munich, Germany.

Kley J and Voigt T (2008) Late Cretaceous intraplate thrusting in Central Europe: effect of Africa-Iberia-Europe convergence, not Alpine collision. *Geology* **36**, 839–42.

Köhler S, Duschl F, Fazlikhani H and Köhn D (2020) Inversion tectonics, intracontinental fold-and-thrust belts and complex stress fields in central Europe: the history of the Franconian Basin revealed by paleostress analysis, geological maps and field observations. *EGU General Assembly Conference Abstracts*, 2020-03-23, p. 2601.

Köhler, S., Duschl, F., Fazlikhani, H., Koehn, D., Stephan, & H., Stollhofen, H. (2022). Reconstruction of cyclic Mesozoic-Cenozoic stress development in SE Germany using fault-slip and stylolite inversion. *Geological Magazine*, **159,** this issue.

Korneva I, Tondi E, Agosta F, Rustichelli A, Spina V, Bitonte R and Di Cuia R (2014) Structural properties of fractured and faulted Cretaceous platform carbonates, Murge Plateau (southern Italy). *Marine and Petroleum Geology* **57**, 312–26.

Koyama T, Li B, Jiang Y and Jing L (2009) Numerical modelling of fluid flow tests in a rock fracture with a special algorithm for contact areas. *Computers and Geotechnics* **36**, 291–303.

Kroner U, Hahn T, Romer RL and Linnemann U (2007) The Variscan orogeny in the Saxo-Thuringian zone: heterogenous overprint of Cadomian/Paleozoic Peri-Gondwana crust. *Geological Society of America Special Papers* **423**, 153–72.

Kurz W, Imber J, Wibberley CAJ, Holdsworth RE and Collettini C (2008) The internal structure of fault zones: fluid flow and mechanical properties. In *The Geodynamics of the Aegean and Anatolia* (eds T Taymaz, Y Yilmaz and Y Dilek), pp. 1–3. Geological Society of London, Special Publication no. 299.

La Bruna V, Bezerra FH, Souza VH, Maia RP, Auler AS, Araujo RE, Cazarin CL, Rodrigues MAF, Vieira MC and Sousa MO (2021) High-permeability zones in folded and faulted silicified carbonate rocks: implications for karstified carbonate reservoirs. *Marine and Petroleum Geology* **128**, 105046.

Lee J and Babadagli T (2021) Effect of roughness on fluid flow and solute transport in a single fracture: a review of recent developments, current trends, and future research. *Journal of Natural Gas Science and Engineering* **91**, 103971.

Lei Q, Latham JP and Tsang CF (2017) The use of discrete fracture networks for modelling coupled geomechanical and hydrological behaviour of fractured rocks. *Computers and Geotechnics* **85**, 151–76.

Lepillier B, Daniilidis A, Gholizadeh ND, Bruna PO, Kummerow J and Bruhn D (2019) A fracture flow permeability and stress dependency simulation applied to multi-reservoirs, multi-production scenarios analysis. *Geothermal Energy* **7**, 1–16.

Lesueur M, Poulet T and Veveakis M (2020) Three-scale multiphysics finite element framework (FE3) modelling fault reactivation. *Computer Methods in Applied Mechanics and Engineering* **365**, 112988.

Li B, Liu R and Jiang Y (2016) Influences of hydraulic gradient, surface roughness, intersecting angle, and scale effect on nonlinear flow behavior at single fracture intersections. *Journal of Hydrology* **538**, 440–53.

Lipsey L, Pluymaekers M, Goldberg T, van Oversteeg K, Ghazaryan L, Cloetingh S and van Wees JD (2016) Numerical modelling of thermal convection in the Luttelgeest carbonate platform, the Netherlands. *Geothermics* **64**, 135–51.

Liu R, Li B and Jiang Y (2016) A fractal model based on a new governing equation of fluid flow in fractures for characterizing hydraulic properties of rock fracture networks. *Computers and Geotechnics* **75**, 57–68.

Lopes JA, Medeiros WE, La Bruna V, de Lima A, Bezerra FH and Schiozer DJ (2022) Advancements towards DFKN modelling: incorporating fracture enlargement resulting from karstic dissolution in discrete fracture networks. *Journal of Petroleum Science and Engineering* **209**, 109944.

Manzocchi T (2002) The connectivity of two-dimensional networks of spatially correlated fractures. *Water Resources Research* **38**, 1162.

Manzocchi T, Childs C and Walsh JJ (2010) Faults and fault properties in hydrocarbon flow models. *Geofluids* **10**, 94–113.

Martin V, Jaffré J and Roberts JE (2005) Modelling fractures and barriers as interfaces for flow in porous media. *SIAM Journal of Scientific Computing* **26**, 1667–91.

Mazur S, Scheck-Wenderoth M and Krzywiec P (2005) Different modes of the Late Cretaceous–Early Tertiary inversion in the North German and Polish basins. *International Journal of Earth Sciences* **94**, 782–98.

Meier T, Grühser C and Backers T (2018) Workflow for homogenising permeability of a low permeable rock containing a high permeable discrete fracture network. In 80th EAGE Conference and Exhibition 2018, 11th–14th June 2018, Copenhagen, Denmark.

Meyer RK and Schmidt-Kaler H (1990) Paläogeographie und Schwammriffentwicklung des süddeutschen Malm: ein Überblick. *Facies* **23**, 175–84.

Mitchell TM and Faulkner DR (2009) The nature and origin of off-fault damage surrounding strike-slip fault zones with a wide range of displacements: a field study from the Atacama fault system, northern Chile. *Journal of Structural Geology* **31**, 802–16.

Morley CK and Nixon CW (2016) Topological characteristics of simple and complex normal fault networks. *Journal of Structural Geology* **84**, 68–84.

Navabpour P, Malz A, Kley J, Siegburg M, Kasch N and Ustaszewski K (2017) Intraplate brittle deformation and states of paleostress constrained by fault kinematics in the central German platform. *Tectonophysics* **694**, 146–63.

Nelson R (2001). *Geologic Analysis of Naturally Fractured Reservoirs*. Oxford: Gulf Professional Publishing.

Nordbotten J, Boon WM, Fumagalli A and Keilegavlen E (2018) Unified approach to discretization of flow in fractured porous media. *Computational Geoscience* **23**, 225–37.

Odling NE, Gillespie P, Bourgine B, Castaing C, Chiles JP, Christensen NP, Fillion E, Genter A, Olsen C, Thrane L and Trice R (1999) Variations in fracture system geometry and their implications for fluid flow in fractured hydrocarbon reservoirs. *Petroleum Geoscience* **5**, 373–84.

Peacock DC, Sanderson DJ, Bastesen E, Rotevatn A and Storstein TH (2019) Causes of bias and uncertainty in fracture network analysis. *Norwegian Journal of Geology* **99**, 113–28.

Permann CJ, Gaston DR, Andrš D, Carlsen RW, Kong F, Lindsay AD, Miller JM, Peterson JW, Slaughter AE, Stogner RH and Martineau RC (2020) MOOSE: enabling massively parallel multiphysics simulation. *SoftwareX* **11**, 100430.

Peterek A, Maier M, Bankwitz P, Franzke H-J, Rauche H and Schröder B (1993) Contribution to the late- and post Variscan tectonic evolution at the western margin of the Bohemian Massif. *KTB-Report* **93–2**, 107–10.

Peterek A, Rauche H and Schröder B (1996) Die strukturelle Entwicklung des E-Randes der Süddeutschen Scholle in der Kreide. *Zeitschrift für geologische Wissenschaften* **24**, 65–77.

Peterek A, Rauche H, Schröder B, Franzke H-J, Bankwitz P and Bankwitz E (1997) The late- and post-Variscan tectonic evolution of the western border fault zone of the Bohemian massif (WBZ). *Geologische Rundschau* **86**, 191–202.

Peterek A and Schröder B (2010) Geomorphologic evolution of the cuesta landscapes around the northern Franconian Alb: review and synthesis. *Zeitschrift für Geomorphologie* **54**, 305–45.

Pisani L, Antonellini M, Bezerra FHR, Carbone C, Auler AS, Audra P, La Bruna V, Bertotti G, Balsamo F, Pontes CCC and de Waele J (2022) Silicification, flow pathways, and deep-seated hypogene dissolution controlled by structural and stratigraphic variability in a carbonate-siliciclastic sequence (Brazil). *Marine and Petroleum Geology* **139**, 105611.

Pontes CC, Bezerra FH, Bertotti G, La Bruna V, Audra P, De Waele J, Auler AS, Balsamo F, De Hoop S and Pisani L (2021) Flow pathways in multiple-direction fold hinges: implications for fractured and karstified carbonate reservoirs. *Journal of Structural Geology* **146**, 104324.

Poulet T, Lesueur M and Kelka U (2021) Dynamic modelling of overprinted low-permeability fault cores and surrounding damage zones as lower dimensional interfaces for multiphysics simulations. *Computers and Geosciences* **150**, 104719.

Poulet T, Paesold M and Veveakis M (2017) Multi-physics modelling of fault mechanics using redback: a parallel open-source simulator for tightly coupled problems. *Rock Mechanics and Rock Engineering* **50**, 733–49.

Prabhakaran R, Bruna PO, Bertotti G, Mittempergher S, Succo A, Bistacchi A and Storti F (2018) Characterizing stress-sensitive fracture apertures in discrete fracture network representations. In AAPG ACE 2018, 20th–23rd May 2018, Salt Lake City, USA.

Prabhakaran R, Bruna PO, Bertotti G and Smeulders D (2019) An automated fracture trace detection technique using the complex shearlet transform. *Solid Earth* **10**, 2137–66.

Prabhakaran R, Bertotti G, Urai J and Smeulders D (2021) Investigating spatial heterogeneity within fracture networks using hierarchical clustering and graph distance metrics. *Solid Earth* **12**, 2159–209.

Priest SD and Hudson JA (1976) Discontinuity spacings in rock. *International Journal of Rock Mechanics and Mining Sciences & Geomechanics Abstracts* **13**, 135–48.

Priest SD and Hudson JA (1981) Estimation of discontinuity spacing and trace length using scanline surveys. *International Journal of Rock Mechanics and Mining Sciences & Geomechanics Abstracts* **18**, 183–97.

Pringle JK, Howell JA, Hodgetts D, Westerman AR and Hodgson DM (2006) Virtual outcrop models of petroleum reservoir analogues: a review of the current state-of-the-art. *First Break* **24**, 33–42.

Przybycin AM, Scheck-Wenderoth M and Schneider M (2017) The origin of deep geothermal anomalies in the German Molasse Basin: results from 3D numerical models of coupled fluid flow and heat transport. *Geothermal Energy* **5**, 1–28.

Rajabi M, Sherkati S, Bohloli B and Tingay M (2010) Subsurface fracture analysis and determination of in-situ stress direction using FMI logs: an example from the Santonian carbonates (Ilam Formation) in the Abadan Plain, Iran. *Tectonophysics* **492**, 192–200.

Rajchl M, Uličný D, Grygar R and Mach K (2009) Evolution of basin architecture in an incipient continental rift: the Cenozoic Most Basin, Eger Graben (Central Europe). *Basin Research* 21, 269–94.

Renard P, Genty A and Stauffer F (2001) Laboratory determination of the full permeability tensor. *Journal of Geophysical Research: Solid Earth* 106, 26443–52.

Rong G, Peng J, Wang X, Liu G and Hou D (2013) Permeability tensor and representative elementary volume of fractured rock masses. *Hydrogeology Journal*, 21, 1655–71. https://doi.org/10.1007/s10040-013-1040-x

Sanderson DJ and Zhang X (2004) Stress-controlled localization of deformation and fluid flow in fractured rocks. In *The Initiation, Propagation, and Arrest of Joints and Other Fractures* (ed JW Cosgrove), pp. 299–314. *Geological Society of London, Special Publication* no. 231.

Saxena A, Nibur K and Prakash A (2018) Applications of fracture mechanics in assessing integrity of hydrogen storage systems. *Engineering Fracture Mechanics* 187, 368–80.

Schäfer F, Oncken O, Kemnitz H and Romer RL (2000) Upper-plate deformation during collisional orogeny: a case study from the German Variscides (Saxo-Thuringian Zone). In *Orogenic Processes: Quantification and Modelling in the Variscan Belt* (eds W Franke, V Haak, O Oncken and D Tanner), pp. 281–302. Geological Society of London, Special Publication no. 179.

Scheck-Wenderoth M, Krzywiec P, Zühlke R, Maystrenko Y and Froitzheim N (2008) Permian to Cretaceous tectonics. In *The Geology of Central Europe Volume 2: Mesozoic and Cenozoic* (ed T McCann), pp. 999–1030. London: Geological Society of London.

Schintgen TV and Moeck IS (2021) The interplay of Malm carbonate permeability, gravity-driven groundwater flow, and paleoclimate – implications for the geothermal field and potential in the Molasse Basin (Southern Germany): a foreland-basin play. *Geothermal Energy* 9, 25 (1–43).

Schröder B (1987) Inversion tectonics along the western margin of the Bohemian Massif. *Tectonophysics* 137, 93–100.

Schröder B, Ahrendt H, Peterek A and Wemmer K (1997) Post-Variscan sedimentary record of the SW margin of the Bohemian massif: a review. *Geologische Rundschau* 86, 178–84.

Sibson RH (1996) Structural permeability of fluid-driven fault-fracture meshes. *Journal of Structural Geology* 18, 1031–42.

Sippel J, Saintot A, Heeremans M and Scheck-Wenderoth M (2010) Paleostress field reconstruction in the Oslo region. *Marine and Petroleum Geology* 27, 682–708.

Sloan R (2003) Quantification of uncertainty in recovery efficiency predictions: lessons learned from 250 mature carbonate fields. In SPE Annual Technical Conference and Exhibition, 5th–8th October 2003, Denver, USA.

Smeraglia L, Giuffrida A, Grimaldi S, Pullen A, La Bruna V, Billi A and Agosta F (2021) Fault-controlled upwelling of low-T hydrothermal fluids tracked by travertines in a fold-and-thrust belt, Monte Alpi, Southern Apennines, Italy. *Journal of Structural Geology* 144, 104276.

Smith RY (2020) Regional geology and fracture network characterisation of the Southern Chotts and Jeffara Basins, Central Tunisia. MSc Thesis. Delft University of Technology, Delft, the Netherlands. Published thesis.

Snow DT (1969) Anisotropic permeability of fractured media. *Water Resources Research* 5, 1273–89.

Stettner G and Salger M (1985) Das Schiefergebirge in der Forschungsbohrung Obernsees. *Geologica Bavarica* 88, 49–55.

Sollhofen H, Bachmann GH, Barnasch J, Bayer U, Beutler G, Franz M, Kästner M, Legler B, Mutterlose J and Radies D (2008) Upper Rotliegend to Early Cretaceous basin development. In *Dynamics of Complex Intracontinental Basins: The Central European Basin System* (eds R Littke and U Bayer), pp. 181–210. Berlin: Springer.

Stork AL, Verdon JP and Kendall JM (2015) The microseismic response at the In Salah Carbon Capture and Storage (CCS) site. *International Journal of Greenhouse Gas Control* 32, 159–71.

Thovert JF, Mourzenko VV and Adler PM (2017) Percolation in three-dimensional fracture networks for arbitrary size and shape distributions. *Physical Reviews* 95, 42–112.

Vidal J, Genter A and Chopin F (2017) Permeable fracture zones in the hard rocks of the geothermal reservoir at Rittershoffen, France, *Journal of Geophysical Research: Solid Earth* 122, 4864–87.

Voigt T, Kley J and Voigt S (2021) Dawn and dusk of Late Cretaceous basin inversion in central Europe. *Solid Earth* 12, 1443–71.

Volatili T, Zambrano M, Cilona A, Huisman BAH, Rustichelli A, Giorgioni M and Tondi E (2019) From fracture analysis to flow simulations in fractured carbonates: the case study of the Roman Valley Quarry (Majella Mountain, Italy). *Marine and Petroleum Geology* 100, 95–110.

Wagner GA, Coyle DA, Duyster J, Henjes-Kunst F, Peterek A, Schröder B, Stöckhert K, Wemmer G, Zulauf G, Ahrendt H, Bischoff E, Hejl E, Jacobs J, Menzel D, Nand L, van den Haute P, Vercoutere C and Welzel B (1997) Post-Variscan thermal and tectonic evolution of the KTB site and its surroundings. *Journal of Geophysical Research: Solid Earth* 102, 18221–32.

Watkins H, Healy D, Bond CE and Butler RW (2018) Implications of heterogeneous fracture distribution on reservoir quality: an analogue from the Torridon Group sandstone, Moine Thrust Belt, NW Scotland. *Journal of Structural Geology* 108, 180–97.

Wawerzinek B, Buness H, von Hartmann H and Tanner DC (2021) S-wave experiments for the exploration of a deep geothermal carbonate reservoir in the German Molasse Basin. *Geothermal Energy* 9, 1–21.

Welch MJ, Souque C, Davies RK and Knipe RJ (2015) Using mechanical models to investigate the controls on fracture geometry and distribution in chalk. In *Fundamental Controls on Fluid Flow in Carbonates: Current Workflows to Emerging Technologies* (eds SM Agar and S Geiger), pp. 281–309. *Geological Society of London, Special Publication* no. 406.

Wibberley CAJ and Shimamoto T (2002) Internal structure and permeability of major strike-slip fault zones: the median tectonic line in Mie prefecture, southwest Japan. *Journal of Structural Geology* 25, 59–78.

Wilkins A, Green CP and Ennis-King J (2021) An open-source multiphysics simulation code for coupled problems in porous media. *Computers and Geosciences* 154, 104820.

Witherspoon PA, Wang JS, Iwai K and Gale JE (1980) Validity of cubic law for fluid flow in a deformable rock fracture. *Water Resources Research* 16, 1016–24.

Witter JB, Trainor-Guitton WJ and Siler DL (2019) Uncertainty and risk evaluation during the exploration stage of geothermal development: a review. *Geothermics* 78, 233–42.

Zeeb C, Gomez-Rivas E, Bons PD and Blum P (2013) Evaluation of sampling methods for fracture network characterization using outcrops. *AAPG Bulletin* 97, 1545–66.

Zhang JJ (2019) Rock physical and mechanical properties. In *Applied Petroleum Geomechanics* (ed JJ Zhang), pp. 29–83. Oxford: Gulf Professional Publishing.

Zhang X, Sanderson DJ, Harkness RM and Last NC (1996) Evaluation of the 2-D permeability tensor for fractured rock masses. *International Journal of Rock Mechanics and Mining Sciences & Geomechanics Abstracts* 33, 17–37.

Zhang Y, Schaubs PM, Zhao C, Ord A, Hobbs BE and Barnicoat AC (2008) Fault-related dilation, permeability enhancement, fluid flow and mineral precipitation patterns: numerical models. In *The Geodynamics of the Aegean and Anatolia* (eds T Taymaz, Y Yilmaz and Y Dilek), pp. 239–55. *Geological Society of London, Special Publication* no. 299.

Ziegler PA (1990) Collision related intra-plate compression deformations in Western and Central Europe. *Journal of Geodynamics* 11, 357–88.

Ziegler PA (1992) European Cenozoic rift system. *Tectonophysics* 208, 91–111.

Zulauf G and Duyster J (1997) Supracrustal intraplate thickening of Variscan basement due to Alpine foreland compression: results from the superdeep well KTB (Bohemian Massif, Germany). *Tectonics* 16, 730–43.